Precambrian Research 298 (2017) 512–529

Contents lists available at ScienceDirect

Precambrian Research

journal homepage: www.elsevier.com/locate/precamres

Acanthomorphic acritarchs of the Doushantuo Formation from an upper slope section in northwestern Hunan Province, South China, with implications for early–middle Ediacaran biostratigraphy

Qing Ouyang [a,b], Chengguo Guan [a], Chuanming Zhou [a,*], Shuhai Xiao [c]

[a] CAS Key Laboratory of Economic Stratigraphy and Palaeogeography, Nanjing Institute of Geology and Palaeontology, Chinese Academy of Sciences, Nanjing 210008, PR China
[b] University of Chinese Academy of Sciences, Beijing 100049, PR China
[c] Department of Geosciences, Virginia Tech, Blacksburg, VA 24061, USA

ARTICLE INFO

Article history:
Received 26 March 2017
Revised 29 June 2017
Accepted 4 July 2017
Available online 6 July 2017

Keywords:
Doushantuo-Pertatataka acritarchs
Upper slope environment
South China
Ediacaran biostratigraphy
Carbon isotope chemostratigraphy
Lithostratigraphy

ABSTRACT

Doushantuo-Pertatataka acritarchs (DPAs) are abundant and well preserved in the Ediacaran Doushantuo Formation in South China. Not only do they provide insights into the marine ecosystem immediately after a Neoproterozoic global glaciation, they also afford us an ideal tool for Ediacaran stratigraphic subdivision and correlation. However, previous reports of DPAs in South China are mostly from the Yangtze Gorges area in intra-shelf basin and from Weng'an in shelf margin environments, while data from localities in slope and basinal facies are lacking. Here we present lithostratigraphy, carbon and strontium isotope chemostratigraphy, and acritarch biostratigraphy of the Doushantuo Formation from an upper slope section at Lujiayuanzi in northwestern Hunan Province, South China. Five DPA genera and eight species are preserved in the Doushantuo Formation chert nodules, with the uppermost two DPA horizons occurring above a $\delta^{13}C$ negative excursion that is correlated with the EN3/Shuram excursion based on integrated litho- and chemostratigraphic correlation. Our new findings reveal a broader temporal and spatial distribution of DPAs in South China, and further support their biostratigraphic potential in the early–middle Ediacaran subdivision and correlation.

1. Introduction

Ediacaran large acanthomorphic microfossils, known as Doushantuo-Pertatataka acritarchs (DPAs) (Narbonne et al., 2012; Zhou et al., 2001, 2007), have gained much attention in the past decades because of their importance in understanding Ediacaran biosphere and biostratigraphy (Chen et al., 2014; Cohen et al., 2009; Golubkova et al., 2010; Grey, 2005; Liu et al., 2013a, 2014a; McFadden et al., 2009; Moczydłowska, 2015; Moczydłowska and Nagovitsin, 2012; Narbonne et al., 2012; Xiao et al., 1998, 2014, 2016; Zhou et al., 2007). Currently available data from South China suggest that at least in the Yangtze Gorges area, DPAs appeared shortly after the termination of the Marinoan global glaciation (Zhou et al., 2007), and disappeared at the horizon yielding a prominent carbon isotopic anomaly (EN3, likely equivalent to the Shuram excursion) in the middle Ediacaran Period (Liu et al., 2014a; Narbonne et al., 2012; Xiao et al., 2016), which represents one of the most pronounced negative carbon isotopic excursions in Earth history (Grotzinger et al., 2011) and has been considered as a potential chemostratigraphic tool for Ediacaran subdivision and global correlation (Xiao et al., 2016). However, biostratigraphic data from Russian Plate hint that DPAs may extend above the Shuram-equivalent horizon (Golubkova et al., 2015). Therefore, it is important to document the full stratigraphic range of DPAs in the Yangtze Block of South China in order to test whether DPAs extend above the Shuram excursion.

In the past few decades, abundant DPAs have been reported from chert nodules and phosphorites of the lower–middle Ediacaran Doushantuo Formation in the Yangtze Block of South China (Fig. 1A) (Liu et al., 2014a,b; McFadden et al., 2009; Xiao, 2004a; Xiao et al., 2014; Zhang et al., 1998; Zhou et al., 2007). Phosphatized microfossils have been reported from many places on the Yangtze block, including Weng'an in central Guizhou Province (Xiao et al., 2014; Yuan and Hofmann, 1998; Zhang et al., 1998), Chadian in southern Shaanxi Province (Zhang et al., 1998), Zhangcunping (McFadden et al., 2009, and references therein) and Baizhu (Zhou et al., 2001, 2004) in western Hubei Province, and Chaoyang in eastern Jiangxi Province (Zhou et al., 2002) (Fig. 2). Silicified microfossils, however, have been mainly obtained

* Corresponding author.
E-mail address: cmzhou@nigpas.ac.cn (C. Zhou).

http://dx.doi.org/10.1016/j.precamres.2017.07.005
0301-9268/

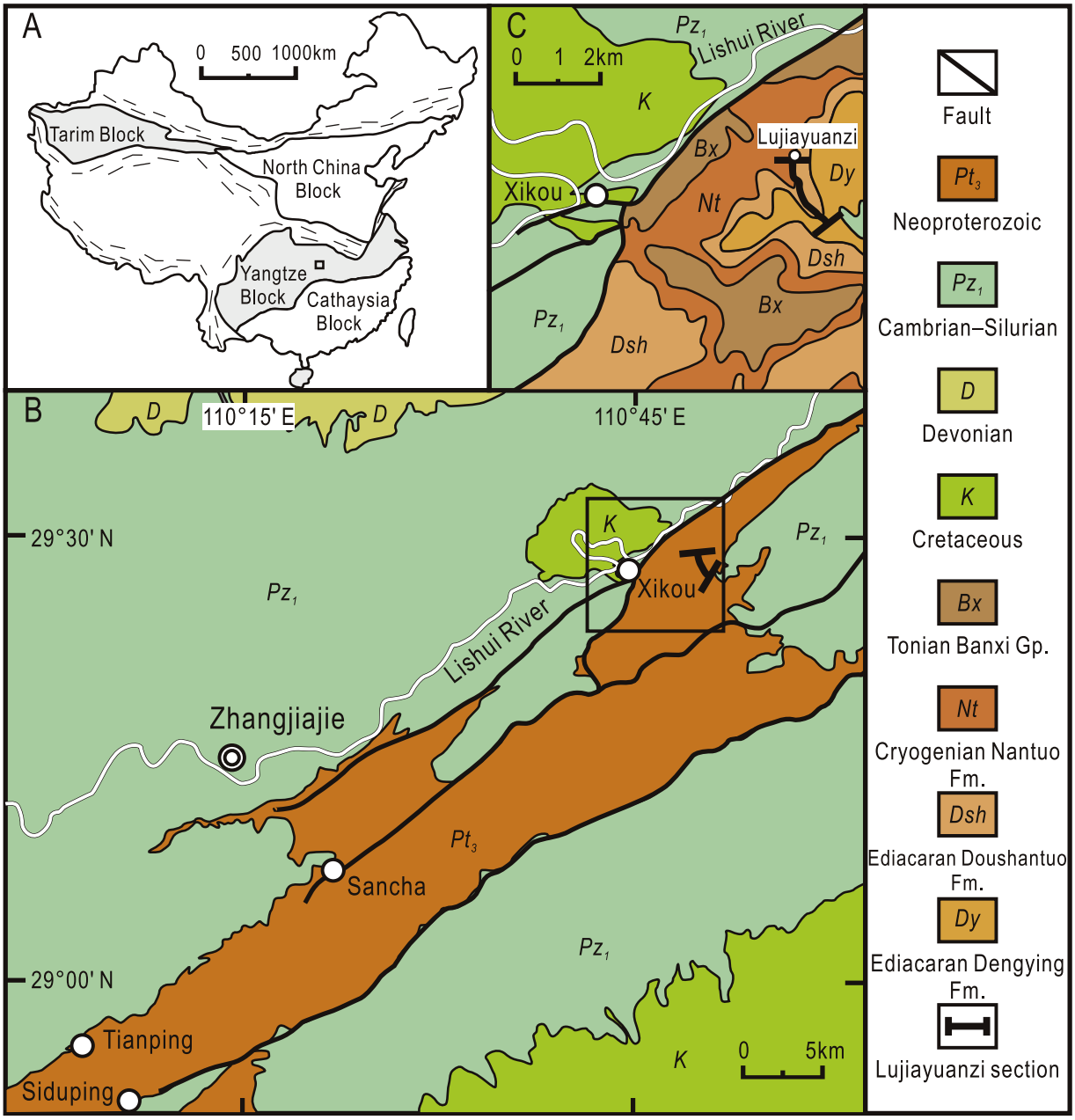

Fig. 1. Geological map. (A) Simplified tectonic map of China, with square marking the location of (B) in the Yangtze Block; (B) Simplified geological map of the Zhangjiajie area, with a square marking the location of (C); (C) Detailed geological map of the Lujiayuanzi section area.

from the Doushantuo chert nodules in the Yangtze Gorges areas of western Hubei Province (Liu et al., 2014b; Xiao, 2004b; Zhang et al., 1998; Zhou et al., 2007). Compared with the phosphatized assemblages that are mostly preserved in reworked clasts and restricted within specific phosphorite horizons, silicified DPAs are generally preserved *in situ* and thus have greater potential in Ediacaran acritarch biostratigraphy (Liu et al., 2013a, 2014a; McFadden et al., 2009; Zhou et al., 2007). For example, in the Yangtze Gorges area, two acanthomorph assemblage zones have been recognized—the *Tianzhushania spinosa* assemblage zone in the lower Doushantuo Formation and the *Hocosphaeridium anozos* assemblage zone in the middle–upper Doushantuo Formation (Liu et al., 2013a, 2014b; McFadden et al., 2009; Xiao et al., 2016; Yin et al., 2011a). The *Tianzhushania spinosa* assemblage zone is absent from early Ediacaran successions in many other continents such as Australia and Siberia (Grey et al., 2003; Liu et al., 2013a, 2014a; Moczydłowska and Nagovitsin, 2012; Narbonne et al., 2012; Xiao et al., 2014). Currently available data indicate that acanthomorphs of the *Hocosphaeridium anozos* assemblage zone do not extend above the Shuram-equivalent negative carbon isotope excursion EN3 in South China (Liu et al., 2014a,b).

Previous attempts to recover DPAs preserved in the chert nodules outside the Yangtze Gorges area in South China have met with limited success. Silicified DPA microfossils have been reported from the slope facies Siduping section (Hawkins et al., 2014), but detailed biostratigraphic data have not been published. Here we report a systematic lithostratigraphic, carbon and strontium isotope chemostratigraphic, and paleontological study on the Ediacaran Doushantuo Formation at Lujiayuanzi section in northwestern Hunan Province, South China. Integrated litho-, chemo-, and biostratigraphic data of the Doushantuo Formation at Lujiayuanzi improve the correlation of the Doushantuo Forma-

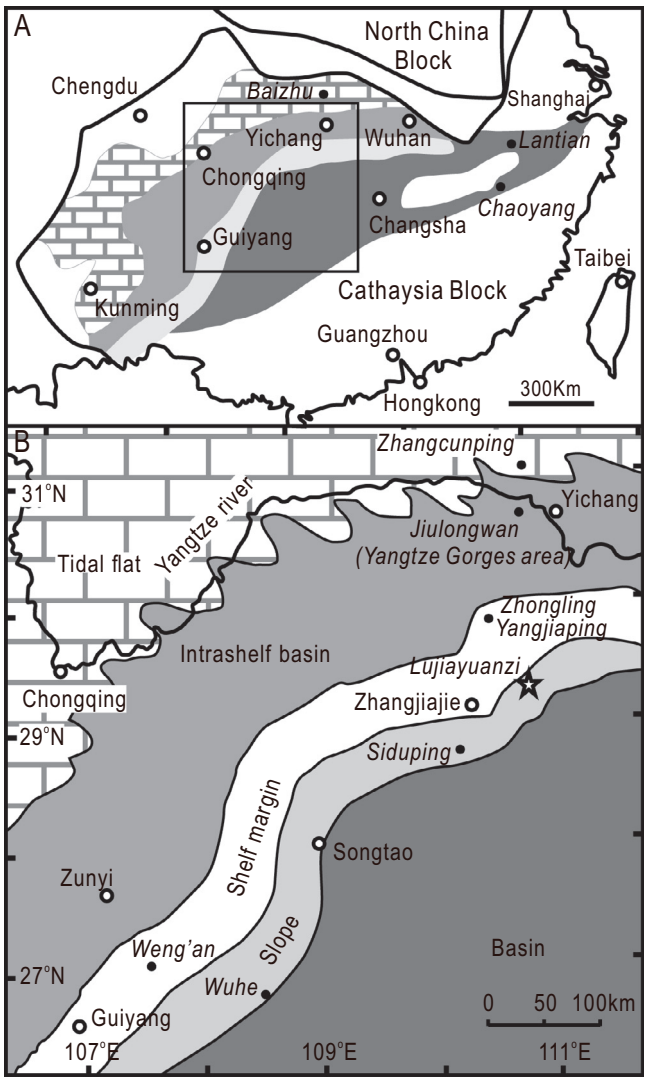

Fig. 2. (A) Paleogeographic map of the Yangtze Block in the early–middle Ediacaran Period. Section localities mentioned in the text are marked, with a square marking the location of (B). (B) Magnified paleogeographic map in the early–middle Ediacaran Period showing the location of the Lujiayuanzi section. Empty circles represent cities/towns, solid circles mark sections (in italic) mentioned in the text, and star marks the Lujiayuanzi section. (A) and (B) are both modified from Jiang et al. (2011).

tion between the upper slope facies and shelf basin in the Yangtze Gorges area. In contrast to previous speculations, the new data suggest that the DPAs continue to exist after the middle Ediacaran EN3/Shuram anomaly.

2. Geological background and stratigraphy of the Doushantuo Formation at Lujiayuanzi

In the Yangtze Block, the Ediacaran succession consists of the Doushantuo and Dengying/Liuchapo formations. The Doushantuo Formation (635 Ma–551 Ma, Condon et al., 2005, but see An et al., 2015 for a different view) is generally characterized by a mixture of siliciclastic and carbonate rocks, with variations in litho-, bio- and chemostratigraphy among sections in different paleogeographic localities (Jiang et al., 2007, 2011; Li et al., 2010; Liu et al., 2013a; Zhou and Xiao, 2007; Zhou et al., 2007; Zhu et al., 2007, 2013).

The Doushantuo Formation in the Yangtze Block was deposited in a passive continental margin that was located in a low–middle latitude area and was adjacent to Australia and/or India (Jiang et al., 2003; Joshi and Tiwari, 2016; Li et al., 1995; Macouin et al., 2004; Zhang et al., 2013). It is widely accepted that this continental margin was a rimmed shelf at least during the depositional stage of the middle–upper Doushantuo Formation, consisting of an intertidal platform in Yunnan and eastern Sichuan provinces, an intra-shelf basin/lagoon in western Hubei, southeastern Chongqing, and northern Guizhou provinces, a shallow water marginal barrier dominated by carbonate and phosphorite stretching from northwestern Hunan to central Guizhou provinces, and a deep water basin in southern Hunan, northern Guangxi and eastern Guizhou provinces (Cao et al., 1989; Jiang et al., 2011; Vernhet and Reijmer, 2010; Zhu et al., 2013) (Fig. 2).

The Lujiayuanzi section (29°13.854′ N, 110°47.710′ E), ~4.5 km to the east of the Xikou Town of the Zhangjiajie City (Fig. 1B, C), was located in the uppermost slope facies (Fig. 2B). In this region, the Neoproterozoic to lowermost Cambrian succession contains the Tonian Banxi Group of metamorphosed sandstone and siltstone with tuffaceous interlayers, the Cryogenian Nantuo Formation, the Ediacaran Doushantuo and Dengying formations, and the Cambrian Niutitang Formation (Zhao et al., 2012). Due to local tectonic activities, hydrothermal quartz and calcite veins are common in this area.

At the Lujiayuanzi section, the Doushantuo Formation is approximately 300 m in thickness, and is dominated by limestone (Figs. 3 and 4A). The lowest unit is a 2.5-m-thick cap carbonate, with the lower 2 m consisting of dolomicrite and recrystallized dolostone intersected by calcite and quartz veins, and the upper 0.5 m consisting of dolomitic limestone rich in pyrite.

Overlying the cap carbonate is a ~60-m-thick interval characterized by calcareous silty shale and argillaceous dolostone (Fig. 5A). Clasts are mostly quartz, feldspar, mica, and phosphatic silts. Chert nodules occur in this interval and further upsection in the Doushantuo Formation. In the upper part of this interval, the strata show strong soft-sediment deformation structures (Fig. 4B).

Further upsection, from 60 m to 120 m, the Doushantuo Formation is composed of micrite and dolomitic micrite (Fig. 5B). At certain horizons, micrite beds are intercalated with argillaceous, organic-rich limestone beds. Recrystallized and vein calcite is common in this unit (Fig. 5C).

Limestone in the 120–185 m interval becomes more argillaceous and organic rich (Fig. 5D). Peloidal layers occur occasionally (Fig. 5E). Above this unit there is a ~60 m interval mainly composed of thin-bedded recrystallized micrite (Fig. 5F), and characterized by large slump structures (Fig. 4C) in the middle–upper part.

The top 40 m of the Doushantuo Formation is dominated by peloidal limestone or dolomitic limestone (Fig. 5G). Small-scaled cross beds occur in this interval (Fig. 4E). Chert nodules or discontinuous cherty bands are abundant (Fig. 4D). This interval is capped by the Doushantuo–Dengying boundary, which is marked by the disappearance of limestone and the first occurrence of massive dolostone (Figs. 4F and 5H).

Despite the occasional occurrence of peloidal limestone, the sparsity of sedimentary structures indicative of high energy hydrodynamic conditions such as cross-beds suggests an overall depositional environment below the fair weather wave base. The lithostratigraphic succession of the Doushantuo Formation includes two shallowing-upward sequences above the cap carbonate unit (Fig. 3). The occurrence of gravity-induced soft-sediment deformation structures in both lower and upper parts of the Doushantuo Formation indicates that this formation was deposited in a slope facies, which is consistent with the paleogeographic reconstruction proposed by Jiang et al. (2011).

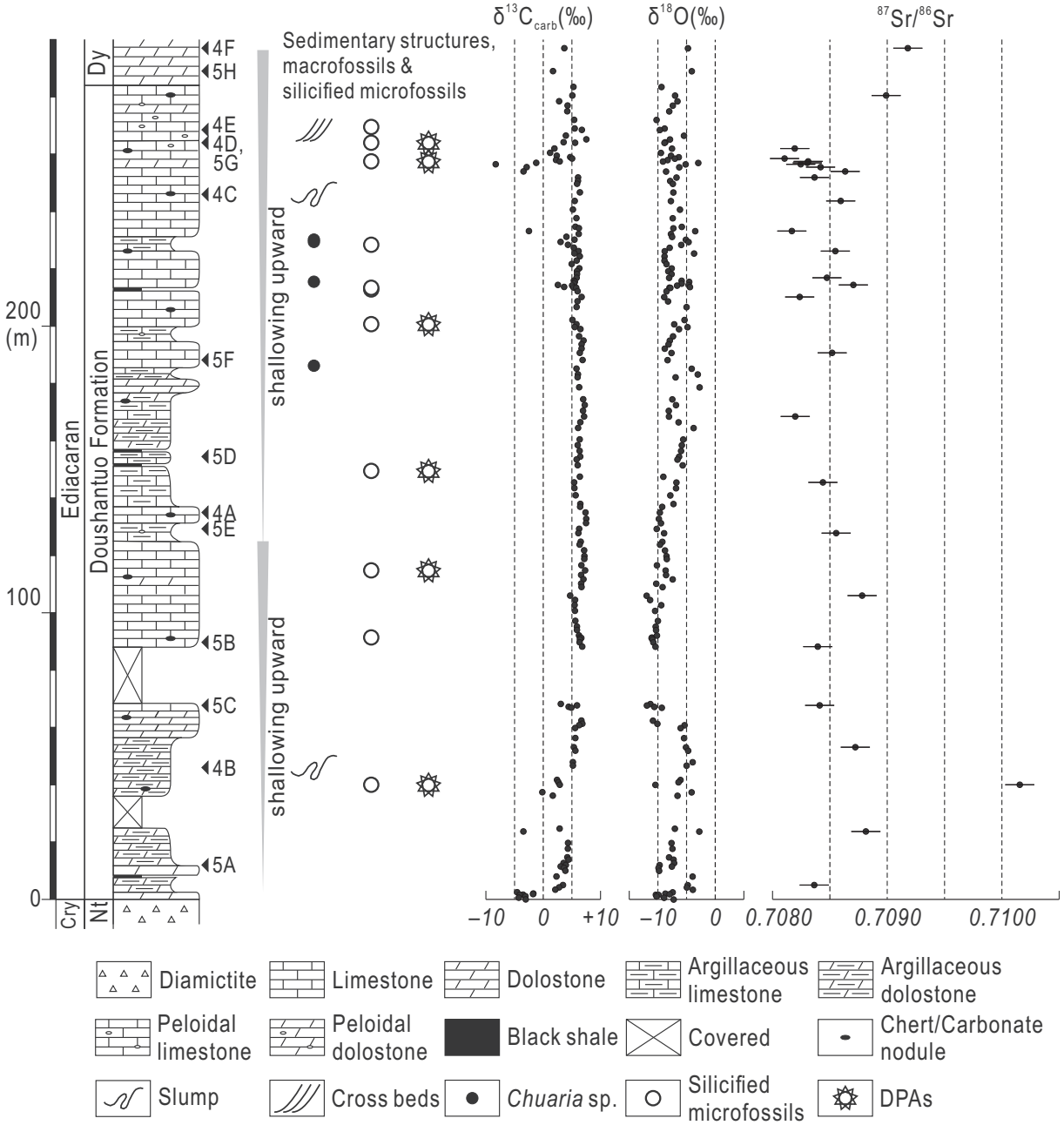

Fig. 3. Lithostratigraphic column, fossil occurrences, and chemostratigraphy of the Lujiayuanzi section. Stratigraphic horizons of the field and thin section photographs in Figs. 4 and 5 are marked in the log. DPAs: Doushantuo-Pertatataka acritarchs. Nt: Nantuo Formation. Dy: Dengying Formation.

3. Materials and methods

Totally 175 rock samples were collected from the Doushantuo Formation and two samples were collected from the basal Dengying Formation (Tables 1 and 2). Thin sections were prepared for petrographic analysis. Chert nodule samples were collected from 18 stratigraphic horizons, and 78 thin sections were made for microfossil investigation (Table 1). All thin sections were carefully examined under a transmitted light microscope.

A total of 164 carbonate samples were prepared for $\delta^{13}C$ and $\delta^{18}O$ analyses in the State Key Laboratory of Palaeobiology and Stratigraphy, Nanjing Institute of Geology and Palaeontology, Chinese Academy of Sciences (NIGPCAS). Powders were micro-drilled from polished slabs to avoid visible veins. An aliquot of 80–100 μg powders of each sample was allowed to react with orthophosphoric acid for 150–200 s at 72 °C in a Kiel IV carbonate device connected to a MAT 253 isotope ratio mass spectrometer. The working standard GBW-04405 was measured to monitor the EA-IRMS system. CO_2 gas calibrated against the NBS19 standard was used as the reference gas. The analytical precision was better than ±0.04‰ for $\delta^{13}C$ and ±0.08‰ for $\delta^{18}O$. Results are reported in the conventional δ-notation versus the VPDB standard (Table 2).

Thirty carbonate samples were selected for element and strontium isotope analyses (Table 2). Approximately 50 mg of micro-drilled powders were dissolved in diluted acetic acid, and the supernatant solution was analyzed for trace element concentrations on an ICP-MS in the Key Laboratory of Economic Stratigraphy and Palaeogeography, NIGPCAS.

Sr isotope measurement followed a two-step leaching technique established by Li et al. (2011). Approximately 0.1 g micro-drilled sample powder was pre-leached by diluted acetic acid and measured for carbonate content. Then, ~50 mg of the powder was lea-

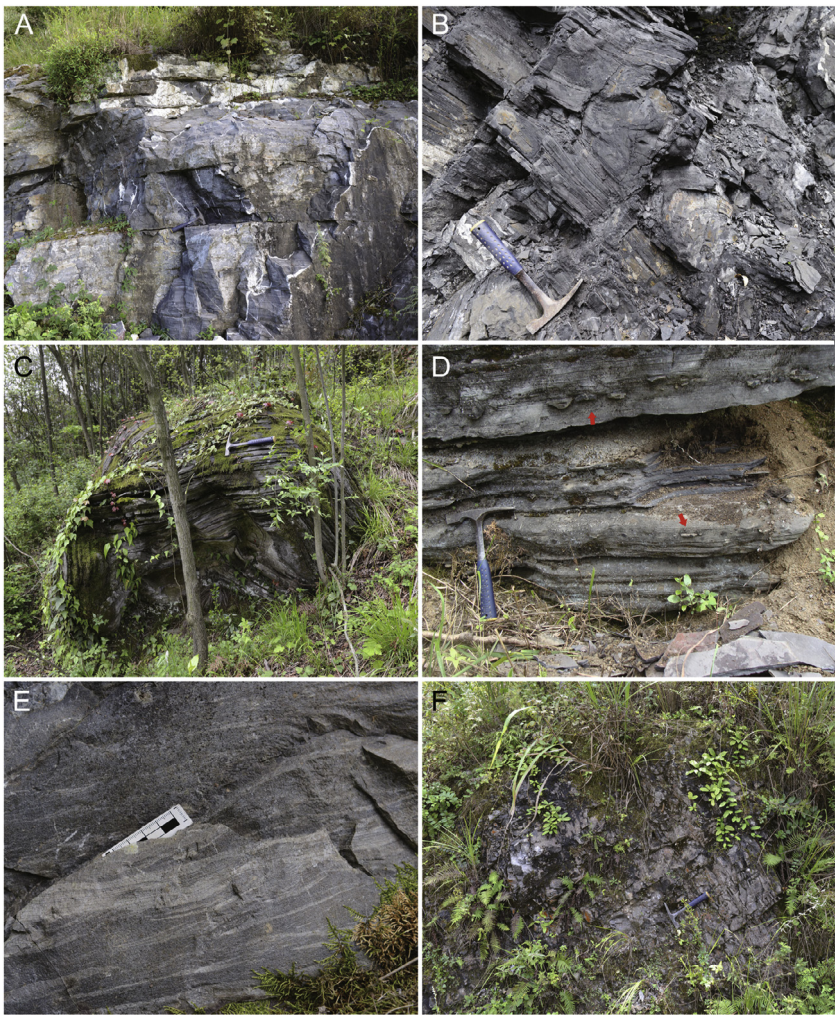

Fig. 4. Outcrop photographs of the Lujiayuanzi section. See Fig. 3 for their horizons. (A) Thick-bedded limestone from the middle Doushantuo Formation; (B) and (C) Slump structures indicative of a slope depositional environment from lower and upper Doushantuo Formation, respectively; (D) Chert nodules (red arrows) from upper Doushantuo Formation; (E) Cross-bedding structure from upper Doushantuo Formation; (F) Dengying Formation dolostone. Rock hammers in A–D and F are ~30 cm long. (For interpretation of the references to colour in this figure legend, the reader is referred to the web version of this article.)

ched twice to dissolve an estimated amount of 30% and 40% carbonate, successively. Sr released from the second leach was dissolved in diluted nitric acid, and was then purified through a cation resin column. The amount of dried purified Sr is consistent with the result of elemental analysis. The re-dissolved Sr was loaded on a tungsten filament for isotopic analysis. Sr isotope ratios were determined on a Triton TIMS (Finnigan Thermo, Germany) in the State Key Laboratory for Mineral Deposits Research, Nanjing University. The recent half-year long-run 2 S.D. of the standard SRM 987 is 0.710244 ± 16 (n = 109). One sample with $^{85}Rb/^{86}Sr$ ratios ≥0.01 was rejected, and among the rest 29 measured samples there were only three that have $^{85}Rb/^{86}Sr$ ratios ≥0.001 (Table 2). The analytical precision was better than ±0.000007. $^{87}Sr/^{86}Sr$ values were not corrected for Rb concentrations.

4. Results and data evaluations

4.1. Paleontological data

Macroscopic (~1–2 mm in diameter) carbonaceous discoidal fossils were discovered from 4 horizons in the upper Doushantuo Formation (Fig. 3). They are 150–550 μm in thickness, bear no concentric folds or other diagnostic structures, and are densely distributed on the bedding surfaces (Fig. 6A). We tentatively identify them as *Chuaria* sp. (Fig. 6B, C).

Microfossils have been discovered from 11 of the 18 chert nodule samples (Table 1), including filamentous and coccoidal prokaryotes, multicellular algae, acanthomorphic acritarchs, and sphaeromorphic acritarchs. These fossils represent taxa previously described from chert nodules of the Doushantuo Formation in South China.

Filamentous cyanobacteria fossils occur from the lowest (~40 m above the base of Doushantuo Formation) to the highest fossiliferous horizon (~269.5 m above the base) (Table 1, Fig. 7H, I), although they are relatively rare and poorly preserved. Most filaments, preserved both as individuals and as clusters, can be assigned to the form genus *Siphonophycus* (Fig. 7I). Considering their high abundance in the Doushantuo Formation chert nodules in the Yangtze Gorges area (Liu et al., 2014b; Zhang et al., 1998), the rare occurrence of filamentous cyanobacteria at Lujiayuanzi may be related to paleoecological or taphonomical factors.

Simple spheroids only occur at two horizons, at 213 m and 269.5 m from the base of the Doushantuo Formation, and they are here tentatively referred to as *Leiosphaeridia* sp. (Fig. 7B). Only one specimen of multicellular alga has been found from a chert nodule at 114.8 m above the base of the Doushantuo Formation (Table 1, Fig. 7A). Despite its incomplete preservation due to the

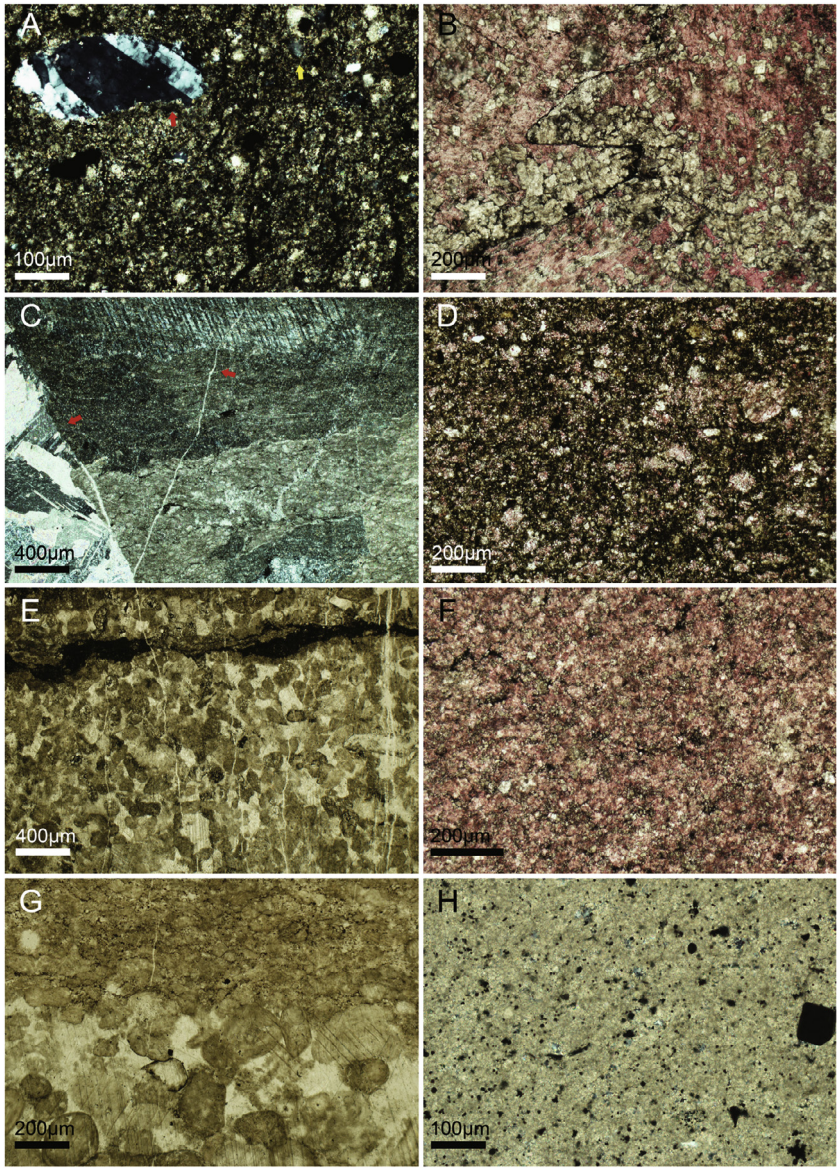

Fig. 5. Thin section photographs under cross-polarized light (XPL) and plane-polarized light (PPL). See Fig. 3 for their horizons. (A) Argillaceous dolostone from the lowermost Doushantuo Formation, showing quartz silt (yellow arrow) and authigenic barite crystals (red arrow). Thin section # 14HA-16, XPL. (B) Dolomitic limestone with a stylolitic structure. Thin section was stained with Alizarin red S. Thin section #14HA-50, PPL. (C) Calcite veins (red arrows) and recrystallized limestone from the lower Doushantuo Formation. Thin section # 14HA-47, XPL. (D) Argillaceous and organic-rich limestone from the lower–middle Doushantuo Formation. Thin section was stained with Alizarin red S. Thin section # 14HA-88, PPL. (E) Clay minerals (the black ribbon), peloids, and thin calcite veins in recrystallized limestone from the lower–middle Doushantuo Formation. Thin section # 14HA-75, XPL. (F) Limestone from the middle-upper Doushantuo Formation. Thin section was stained with Alizarin red S. Thin section # 14HA-107-10, PPL. (G) Peloidal limestone from the uppermost Doushantuo Formation. Thin section #14HA-140, PPL. (H) Dolomicrite of the Dengying Formation with abundant pyrite. Thin section # 14HA-131, XPL. (For interpretation of the references to colour in this figure legend, the reader is referred to the web version of this article.)

truncation of a calcite crystal, its linearly aligned cuboidal cells are a diagnostic feature of *Wengania globosa*, which has been interpreted as stem group florideophytes (Xiao et al., 2004).

Acanthomorphs are present at 5 horizons ranging from 40 m to 264 m above the base of the Doushantuo Formation. In total 26 specimens of spiny acritarchs have been recognized, and 23 of them are identifiable at least to the genus level (Table 1). These spiny acritarchs represent 5 genera and 8 species, according to taxonomic treatments of Grey (2005), Liu et al. (2014b), Moczydłowska (2005), Moczydłowska and Nagovitsin (2012), and Xiao et al. (2014).

The lowest acanthomorph-bearing sample yielded only one acritarch specimen identified as ?*Cavaspina basiconica*. It has a spherical vesicle with relatively short spines that are hollow and freely communicate with vesicle interior (Fig. 8A–C). Some processes have small triangle deflated bases, whereas others taper gradually (Fig. 8B, C), making it difficult to determine whether the basal expansion is a taphonomic artifact. The genus *Cavaspina* and its type species *C. basiconica* were both considered as junior synonyms of *Meghystrichosphaeridium*, *Goniosphaeridium*, and *Gyalosphaeridium* (Grey, 2005; Zhang et al., 1998), but here we follow Moczydłowska (2005) and Xiao et al. (2014) in retaining this genus and its type species.

One highly deformed specimen was observed at 149.5 m (Fig. 8D–F). The size of this specimen is estimated to be 200–500 μm in diameter. Despite the poor preservation, its hollow, thin, almost cylindrical and densely distributed processes (Fig. 8E, F) resemble those of *Appendisphaera*, and comparison with described *Appendisphaera* species suggests an assignment to *A. fragilis*. This specimen is somewhat similar to Ediacaran acanthomorphic acri-

Table 1
Microfossil occurrence at the Lujiayuanzi section.

Sample	Height (m)*	Number of thin sections	DPA											Filamentous and coccoidal fossils	Multicellular algae
			Appendisphaera fragilis	*?Cavaspina basiconica*	*Knollisphaeridium maximum*	*Knollisphaeridium* sp. indet.	*Mengeosphaera chadianensis*	*M. chadianensis?*	*M.? cuspidata*	*M. latibasis?*	*M. spicata?*	*Mengeosphaera* sp. indet.	*Urasphaera fungiformis*	Indeterminate acanthomorphs	Sphaeromorphs		
15HA-13	269.5	4														n/a	
15HA-12	269	1															
15HA-10	264.2	2															
14HA-140	264	5			8	5	1	1	2			1		2			
15HA-6	258.5	5															
15HA-4	257.5	5												1			
15HA-31	228.4	5													n/a		
14HA-125	214.2	5															
14HA-124	213.5	5															
14HA-123	213.4	5													n/a		
14HA-122	213.3	5															
14HA-121	212.8	5								1	1				n/a	n/a	
14HA-115	200.7	3											1			n/a	
14HA-114	199.7	5															
14HA-85	149.5	5	1														1
14HA-67	114.8	5															
14HA-53	91.4	5														n/a	
14HA-30	40	3		1												n/a	

* Stratigraphic height was measured from the base of the Doushantuo Formation; n/a denotes taxa that are present but whose abundance are not available.

tarchs from the Baklia Formation in Svalbard described by Knoll (1992) as *Ericiasphaera spjeldnaesii*. Although the Svalbard specimens were said to have solid processes, they appear to bear thin hollow processes, and a re-examination of the specimens at higher magnification is needed to confirm the nature of their processes.

Three well-preserved acanthomorph specimens were discovered at 200.7 m. The best-preserved specimen is characterized by processes with a distally expanded and truncated termination and a constricted waist just below the distal expansion. This specimen is assigned to *Urasphaera fungiformis* based on the morphology of the processes, including their proportionate length, basal width, and uniformity in process shape (Fig. 8G–J). The specimen is broadly similar to *Briareus borealis*, whose processes are also distally and basally expanded (Knoll, 1992). However, as pointed out by Liu et al. (2014b), the processes of *Briareus borealis* are shorter, much more closely spaced, and have a weakly developed waist.

Two specimens from 200.7 m are assigned to *Mengeosphaera* on the basis of their prominently biform processes. One of them is tentatively identified as *M. latibasis*?, which has a large vesicle bearing processes with obtusely inflated basal expansion supporting a long and thin apical end (Fig. 8K–N). The taxonomic identification is tentative because compared with the *M. latibasis* specimens described by Liu et al. (2014b), our specimen is a little larger, and the height/width ratio of basal expansion is also relatively higher. The other specimen is tentatively identified as *M. spicata*?, which has a small vesicle bearing relatively large and densely distributed processes with an inflated basal expansion (Fig. 8O, P). The taxonomic identification is tentative because the diagnosis of this species requires its processes with a basal expansion longer than wide and an apical end that tapers to a blunt end (Liu et al., 2014b), but neither of the two features can be found in our specimen.

One poorly preserved acanthomorphic acritarch was discovered at 257.5 m. It resembles the genus *Xenosphaera* in its thin and hollow processes (Fig. 7C–E), although most processes preserve only the basal part, and the specimen is much larger than *X. liantuoensis*, the only species of *Xenosphaera*. Thus, we refrain from a formal taxonomic assignment for this specimen.

The highest acanthomorph-bearing bed is relatively more fossiliferous. Twenty acanthomorphic acritarch specimens were discovered, thirteen of which are assigned to the genus *Knollisphaeridium* and five to the genus *Mengeosphaera*. Eight *Knollisphaeridium* specimens are identified as *K. maximum* based on their gradually tapering conical processes that are simple in shape (Fig. 9A–H). The other five specimens are poorly preserved and cannot be identified at the species level. The five *Mengeosphaera* specimens are quite similar to each other. However, following the taxonomic classification for *Mengeosphaera* established by Liu et al. (2014b) and Xiao et al. (2014), we tentatively classified four of them as *M. chadianensis* (Fig. 9L, M) and *M*? *cuspidata* (Fig. 9I–K), whereas the fifth remains unidentifiable at the species level (Table 1). An indeterminate specimen was also discovered from this horizon (Fig. 7F, G). This specimen resembles *Mengeosphaera minima* and *Tanarium elegans* in its small vesicle, as well as the density and basal width of its processes. However, no biform process can be observed from this specimen, and its processes are too short compared with those of *T. elegans*. Thus, no taxonomic identification is given for this specimen. The last specimen found at this horizon is poorly preserved with only three processes visible.

Our observation suggests that larger forms (e.g., *Knollisphaeridium* and *Mengeosphaera*) are preserved much better than smaller ones (e.g., most filamentous and coccoidal microfossils), and acanthomorphs with more robust processes are usually better preserved, indicating that small microfossils are subject to taphonomic destruction due to diagenetic recrystallization of chert nodules.

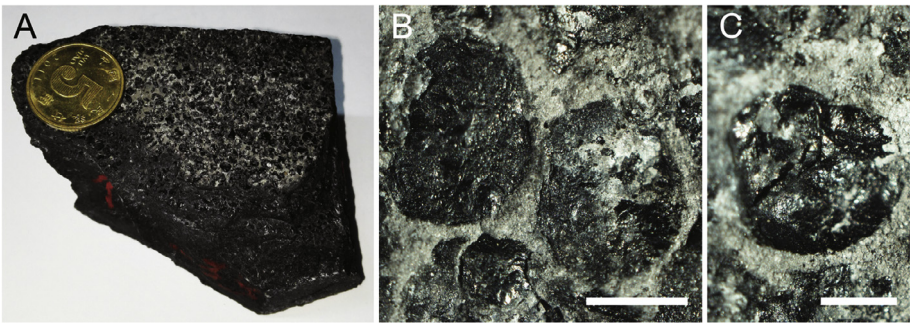

Fig. 6. *Chuaria* sp. fossils from the upper Doushantuo Formation at the Lujiayuanzi section. (A) Fossils are densely distributed on the bedding surface to form a carbonaceous layer. (B) and (C), Close-up views of individual *Chuaria* sp. specimens. Coin in A is 2 cm in diameter. Scale bars in B and C represent 1 mm.

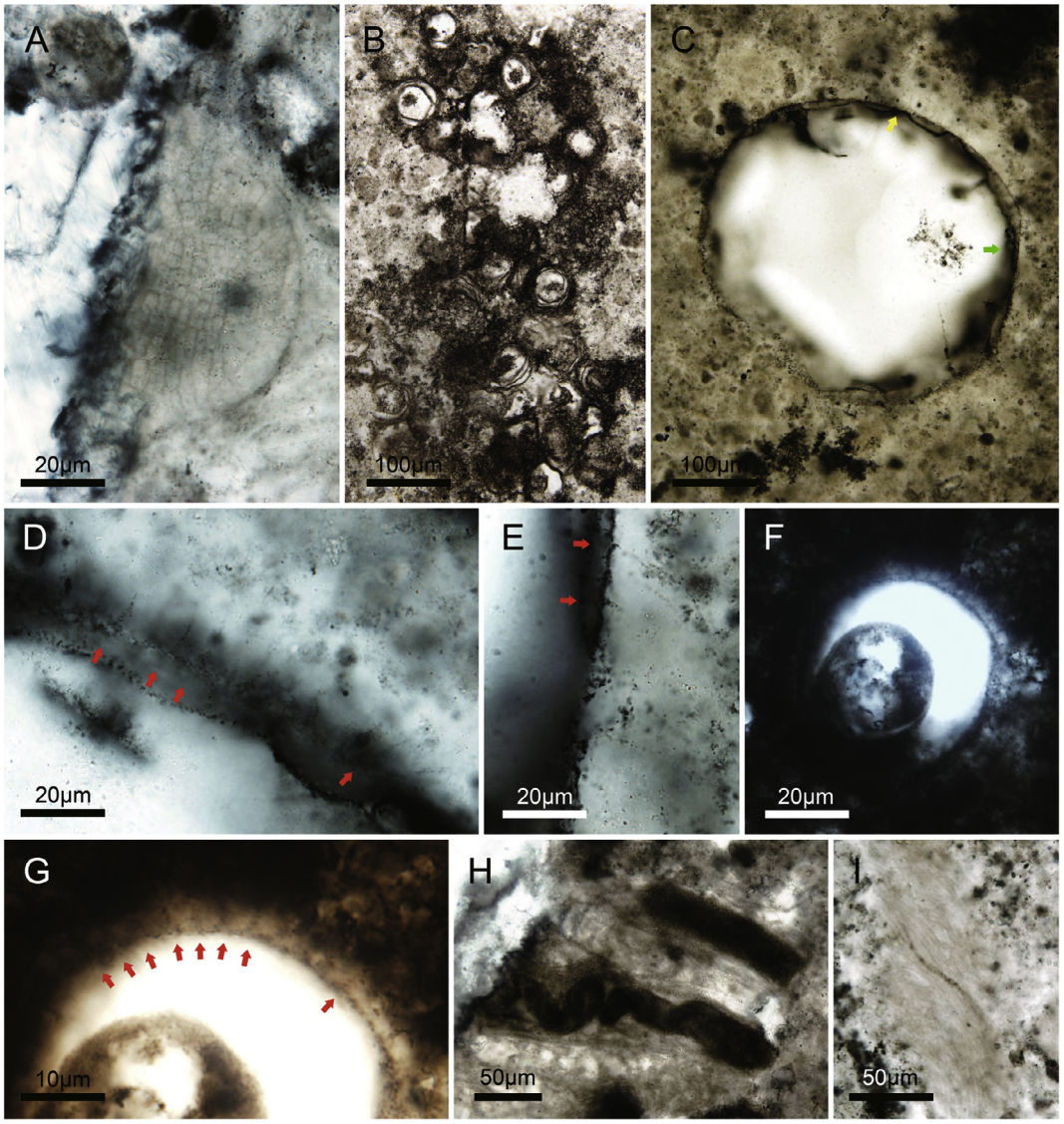

Fig. 7. Silicified microfossils from the Doushantuo Formation at the Lujiayuanzi section. (A) *Wengania globosa*, thin section # 14HA-67-2, Q43/2. (B) Leiospheres, thin section # 14HA-121-3, E34/1. (C)–(E) Poorly preserved acanthomorphic acritarch, thin section # 15HA-4-2, N45/3. (D) and (E), magnified views of (C), marked by the yellow and the green arrows, respectively. Red arrows in (D) and (E) denote thin and hollow conical processes with small expansions at base. (F) and (G) Indeterminate acanthomorphic acritarch, thin section # 14HA-140-2, O32/1. (G) Magnified views of (F). Red arrows denote the short conical processes. (H) Filamentous microfossil, thin section # 14HA-115-2, M43. (I) *Siphonophycus typicum* cluster, thin section # 15HA-13-2, T52/4. All photographs were taken under a transmitted light microscope. All specimens are reposited in NIGPCAS. (For interpretation of the references to colour in this figure legend, the reader is referred to the web version of this article.)

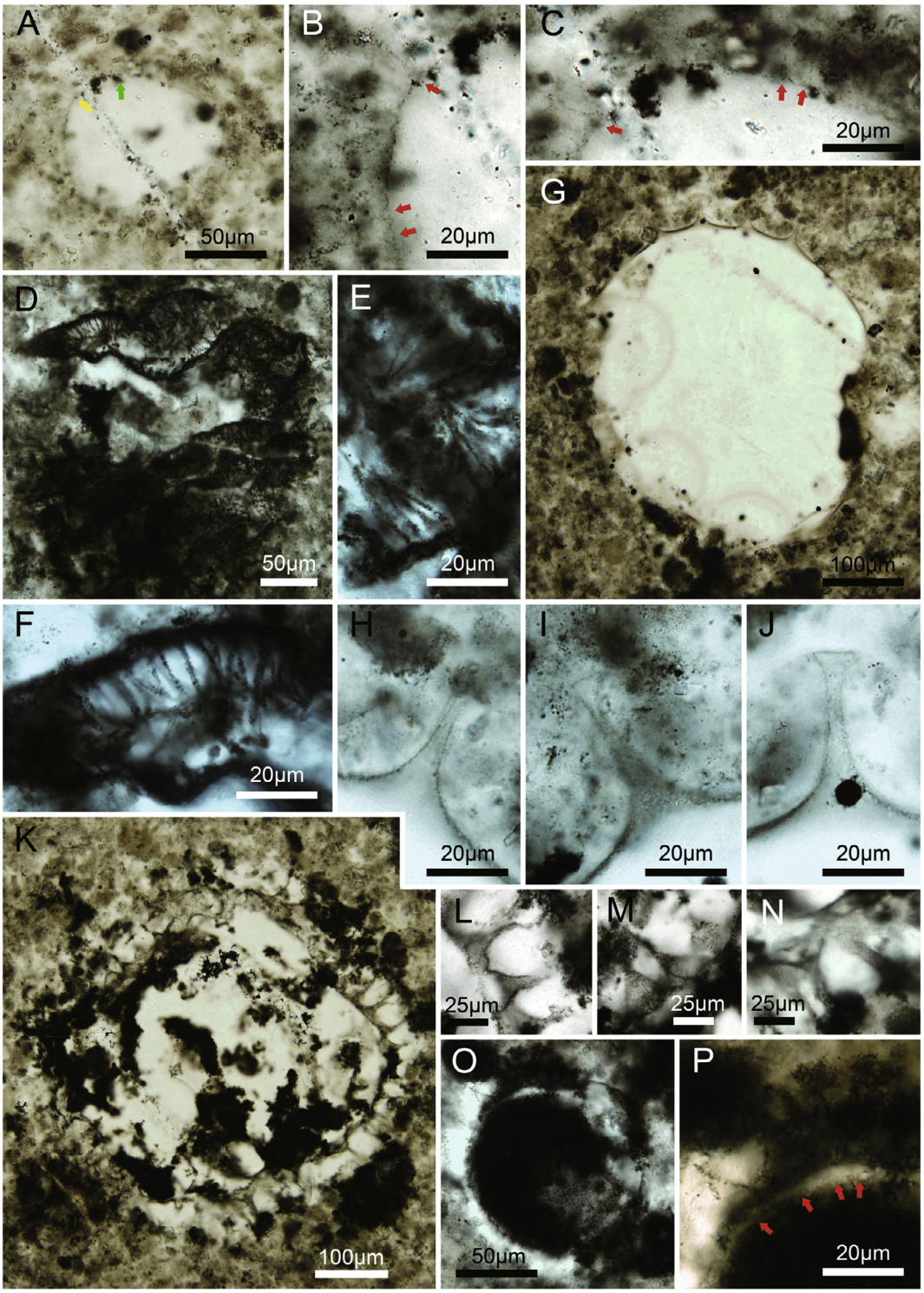

Fig. 8. Silicified microfossils from the Doushantuo Formation at the Lujiayuanzi section. (A)–(C) ?*Cavaspina basiconica*, thin section # 14HA-30-3, P36/2. (B) and (C), magnified views of (A), marked by the yellow and the green arrows, respectively. Red arrows in (B)–(C) denote thin and short conical processes. (D)–(F) Specimen tentatively identified as *Appendisphaera fragilis*, thin section # 14HA-85-5, V46/2. (E) and (F), magnified views of (D) showing densely distributed ciliate processes. (G)–(J) *Urasphaera fungiformis*, thin section # 14HA-115-1, O26. (H)–(J), magnified views of (G) showing apical expansion of conical processes. (K)–(N) *Mengeosphaera latibasis*?, thin section # 14HA-115-1, H27/1. (L)–(N), magnified views of (K) with red arrows showing biform processes with inflated basal expansion and thin apical spine. (O) and (P) *Mengeosphaera spicata*?, thin section # 14HA-115-2, D33. (P), magnified view of (O) showing gradual tapering of biform processes (red arrows). All photographs were taken under a transmitted light microscope. All specimens are reposited in NIGPCAS. (For interpretation of the references to colour in this figure legend, the reader is referred to the web version of this article.)

4.2. Carbon, oxygen, and strontium isotopic data

$\delta^{13}C$, $\delta^{18}O$, and $^{87}Sr/^{86}Sr$ measurements, as well as Mn, Sr, and carbonate contents are summarized in Table 2 and illustrated in Fig. 3.

For most part of the Doushantuo Formation (40–250 m) the $\delta^{13}C$ values are relatively constant at approximately +5‰ (Fig. 3). Two intervals with negative value are observed in the basal and upper parts of the Doushantuo Formation. The basal negative excursion is largely in the cap carbonate, with a nadir of −4.6‰

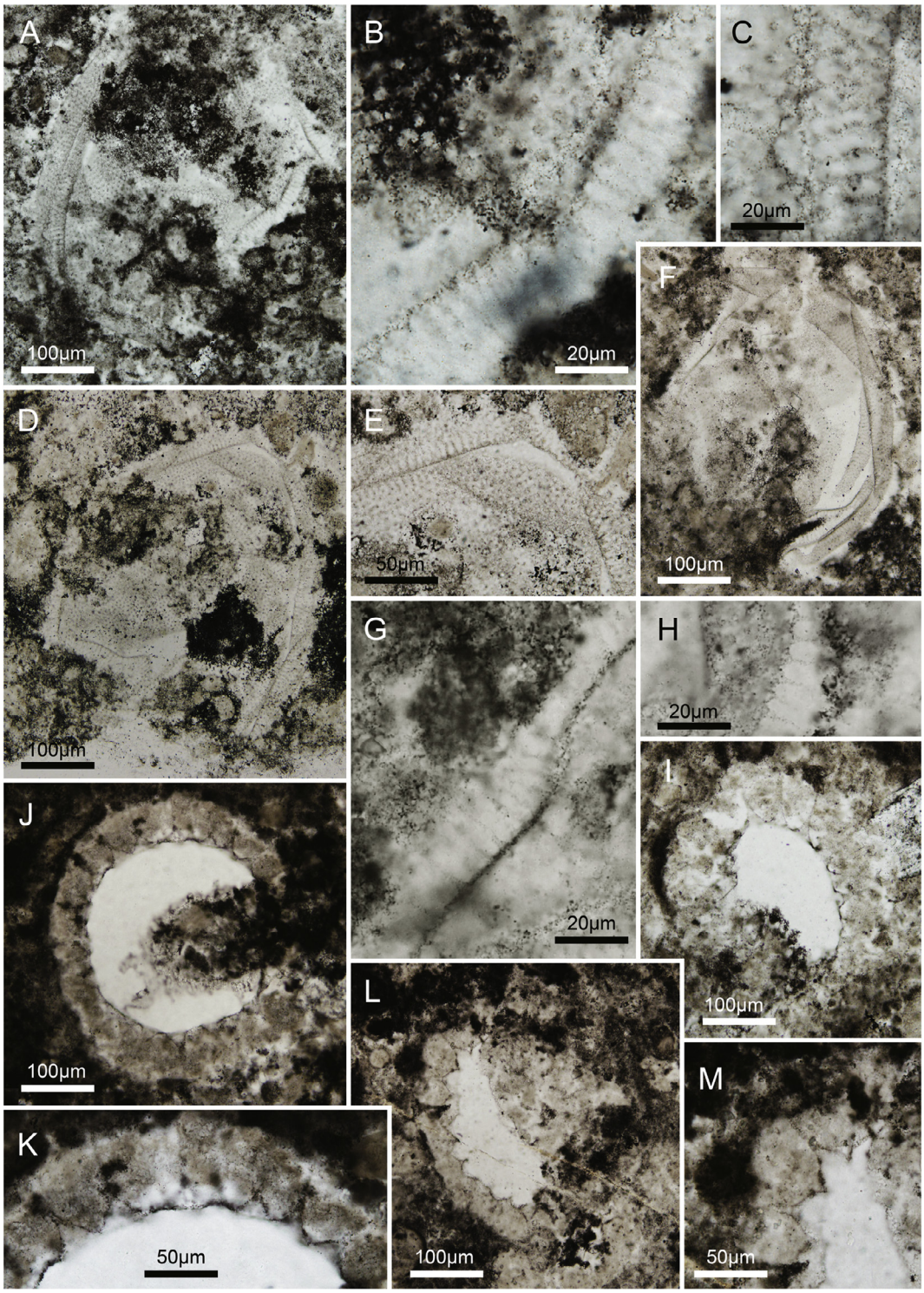

Fig. 9. Silicified microfossils from the Doushantuo Formation at the Lujiayuanzi section. (A)–(H), *Knollisphaeridium maximum*. (A) is from thin section # 14HA-140-1, H25/2. (B) and (C), magnified views of (A). (D) and (F) are from thin section # 14HA-140-3, W48/1 for D and U46/4 for F. (E) magnified view of (D). (G) and (H), magnified view of (F). All magnified photomicrographs show long, simple, and distally tapering processes. (I) *Mengeosphaera*? *cuspidata*, thin section # 14HA-140-1, F56. (J) and (K) *Mengeosphaera*? *cuspidata*, thin section # 14HA-140-5, V52. (K), magnified view of (J) showing biform processes with a deflated conical base supporting a distally tapering spine. (L) and (M) *Mengeosphaera chadianensis*, thin section # 14HA-140-4, V45/2. (M) magnified view of (L) showing biform processes with an inflated basal expansion. All photographs were taken under a transmitted light microscope. All specimens are reposited in NIGPCAS.

at 2.5 m. In the upper part of the Doushantuo Formation, $\delta^{13}C$ values show more frequent fluctuations, with the lowest $\delta^{13}C$ value down to −8.3‰ at 254–257 m (Fig. 3).

Oxygen isotopic composition is more sensitive to post-depositional alteration compared with carbon isotopic composition, because it is less buffered against fluid–rock interactions. Thus, $\delta^{18}O$ values and $\delta^{13}C$–$\delta^{18}O$ covariations, along with trace element concentrations, can be used as an indicator of diagenetic alteration. At the Lujiayuanzi section, most of $\delta^{18}O$ values are higher than −10‰, and there is no positive correlation between

Table 2
Geochemical data of studied samples from the Lujiayuanzi section

Sample	Formation	Height (m)*	Lithology	Carbonate content (%)	$\delta^{13}C_{PDB}$	$\delta^{18}O_{PDB}$	$^{87}Sr/^{87}Sr$	$^{87}Rb/^{87}Sr$	Mn (ppm)	Sr (ppm)	Mn/Sr
14HA-130	Dengying	297	Dolostone	73.10	3.7	−4.8	0.709180	0.000461	374.56	563.84	0.66
14HA-131	Dengying	289	Dolostone		1.7	−4.1					
14HA-132	Doushantuo	283.5	Dolomitic limestone		5.3	−9.4					
14HA-133	Doushantuo	280.5	Calcitic dolostone	95.60	5.1	−7.0	0.708991	0.000361	127.12	763.74	0.17
14HA-134	Doushantuo	278.5	Calcitic dolostone		2.8	−6.6					
14HA-135	Doushantuo	277	Limestone		4.3	−7.4					
14HA-136	Doushantuo	275	Dolomitic limestone		4.2	−8.0					
14HA-137	Doushantuo	272	Limestone		5.4	−10.2					
15HA-12	Doushantuo	269	Limestone		5.5	−8.8					
14HA-138	Doushantuo	268.5	Dolomitic limestone	97.00	6.7	−9.7	0.709134	0.010499	166.18	1018.18	0.16
14HA-139	Doushantuo	266.5	Limestone		4.0	−5.4					
15HA-11	Doushantuo	265.2	Limestone		7.5	−7.9					
15HA-10	Doushantuo	264.2	Calcareous mudstone		3.6	−8.7					
14HA-140	Doushantuo	264	Limestone		5.6	−8.8					
15HA-9	Doushantuo	262	Dolomitic limestone	99.10	2.0	−7.5	0.708194	0.000792	51.13	1891.35	0.03
15HA-8	Doushantuo	260.5	Dolomitic limestone		1.2	−9.5					
15HA-7	Doushantuo	259.5	Dolomitic limestone		2.4	−7.7					
14HA-141	Doushantuo	259	Argillaceous dolostone		4.7	−6.4					
15HA-6	Doushantuo	258.5	Calcitic dolostone	94.40	5.0	−7.0	0.708105	0.000384	107.20	4840.60	0.02
15HA-5	Doushantuo	258	Argillaceous limestone		2.2	−8.3					
15HA-4	Doushantuo	257.5	Limestone	54.40	2.9	−9.1	0.708311	0.000471	132.38	2492.54	0.05
15HA-3	Doushantuo	257	Dolostone	71.20	−1.2	−3.0	0.708303	0.000651	318.46	1459.71	0.22
15HA-2	Doushantuo	256.5	Calcitic dolostone	90.00	−8.3	−5.2	0.708246	0.000957	113.32	3284.72	0.03
14HA-142	Doushantuo	255.5	Brecciated limestone	67.70	−2.9	−6.3	0.708419	0.000263	104.34	2065.00	0.05
15HA-1	Doushantuo	254	Limestone	93.10	−3.4	−8.6	0.708634	0.000710	263.36	4210.86	0.06
15HA-45	Doushantuo	251.9	Dolomitic limestone	93.60	6.1	−6.8	0.708366	0.000615	85.62	8897.44	0.01
15HA-44	Doushantuo	250.7	Dolomitic limestone		6.1	−7.9					
15HA-43	Doushantuo	249.7	Dolomitic limestone		5.9	−7.4					
15HA-42	Doushantuo	246.7	Dolomitic limestone		6.4	−7.3					
15HA-41	Doushantuo	243.7	Dolomitic limestone	94.90	5.5	−7.7	0.708595	0.000573	121.82	4467.94	0.03
15HA-40	Doushantuo	240.7	Dolomitic limestone		5.2	−6.1					
15HA-39	Doushantuo	237.7	Dolomitic limestone		5.8	−7.4					
15HA-38	Doushantuo	234.7	Dolomitic limestone		5.6	−5.8					
15HA-37	Doushantuo	234.2	Limestone		6.2	−7.3					
15HA-36	Doushantuo	233.2	Dolostone	72.10	−2.5	−3.5	0.708168	0.000620	228.24	3408.78	0.07
15HA-34	Doushantuo	232.2	Dolomitic limestone		6.2	−7.7					
15HA-35	Doushantuo	231.2	Dolomitic limestone		4.1	−7.5					
15HA-33	Doushantuo	230.2	Argillaceous limestone		5.5	−5.1					
15HA-32	Doushantuo	229.4	Argillaceous limestone		3.0	−4.6					
15HA-31	Doushantuo	228.4	Argillaceous limestone		4.3	−5.9					
15HA-30	Doushantuo	227.4	Argillaceous limestone		5.3	−7.9					
15HA-29	Doushantuo	226.2	Limestone	97.60	6.2	−8.8	0.708548	0.000211	85.27	7976.69	0.01
15HA-28	Doushantuo	225.4	Limestone		5.5	−3.7					
15HA-27	Doushantuo	224.4	Limestone		6.4	−8.8					
15HA-26	Doushantuo	222.9	Limestone		5.8	−8.8					
15HA-25	Doushantuo	221.7	Limestone		5.0	−8.5					
15HA-24	Doushantuo	220.2	Limestone		6.3	−7.6					
15HA-23	Doushantuo	219.2	Limestone		5.9	−8.2					
15HA-22	Doushantuo	218.2	Limestone		5.9	−7.6					
15HA-21	Doushantuo	216.9	Limestone	94.60	5.8	−8.0	0.708474	0.000171	105.35	4250.62	0.02
15HA-20	Doushantuo	215.9	Limestone		5.3	−5.9					
15HA-19	Doushantuo	215.5	Limestone		5.5	−4.5					
14HA-128	Doushantuo	214.9	Argillaceous limestone		5.4	−5.9					
14HA-127	Doushantuo	214.4	Argillaceous limestone	81.60	2.6	−4.6	0.708705	0.000929	208.39	3733.49	0.06
14HA-125	Doushantuo	214.2	Argillaceous limestone		5.0	−6.6					
14HA-126	Doushantuo	213.7	Argillaceous limestone		3.7	−4.4					
14HA-124	Doushantuo	213.5	Argillaceous limestone		5.3	−8.0					
14HA-123	Doushantuo	213.4	Dolomitic limestone		5.8	−7.8					
14HA-120	Doushantuo	212.2	Dolomitic limestone		6.0	−8.5					
14HA-119	Doushantuo	210.2	Dolomitic limestone	95.40	6.7	−8.9	0.708237	0.000593	64.59	7561.85	0.01
14HA-118	Doushantuo	208.7	Dolomitic limestone		6.0	−8.2					
14HA-117	Doushantuo	206.7	Argillaceous dolostone		5.8	−5.0					
14HA-116	Doushantuo	202.2	Limestone		5.1	−5.4					
14HA-115	Doushantuo	200.7	Dolomitic limestone		5.8	−7.1					
14HA-114	Doushantuo	199.7	Dolomitic limestone		5.5	−4.8					
14HA-113	Doushantuo	199	Argillaceous limestone		6.5	−6.3					
14HA-112	Doushantuo	196.5	Argillaceous limestone		6.3	−7.4					
14HA-111	Doushantuo	195	Argillaceous limestone		7.0	−7.9					
14HA-110	Doushantuo	193.7	Dolomitic limestone		6.7	−8.1					
14HA-109	Doushantuo	192.2	Dolomitic limestone		6.7	−8.8					
14HA-108	Doushantuo	190.7	Dolomitic limestone	92.40	6.4	−7.6	0.708520	0.000765	64.92	13312.51	0.01
14HA-107	Doushantuo	188.2	Dolomitic limestone		6.9	−8.3					
14HA-104	Doushantuo	185.2	Argillaceous limestone		5.8	−4.1					

Table 2 (*continued*)

Sample	Formation	Height (m)*	Lithology	Carbonate content (%)	$\delta^{13}C_{PDB}$	$\delta^{18}O_{PDB}$	$^{87}Sr/^{87}Sr$	$^{87}Rb/^{87}Sr$	Mn (ppm)	Sr (ppm)	Mn/Sr
14HA-103	Doushantuo	183.2	Argillaceous dolostone		6.1	−3.0					
14HA-102	Doushantuo	182.2	Argillaceous dolostone		6.0	−6.9					
14HA-100	Doushantuo	178.7	Dolostone		6.3	−2.7					
14HA-98	Doushantuo	174.5	Argillaceous limestone		7.0	−7.5					
14HA-97	Doushantuo	172.5	Argillaceous limestone		7.3	−6.8					
14HA-96	Doushantuo	170.5	Argillaceous limestone		7.0	−8.1					
14HA-95	Doushantuo	168.5	Argillaceous dolostone	90.80	7.1	−8.1	0.708198	0.000430	132.88	12571.13	0.01
14HA-94	Doushantuo	166.5	Argillaceous dolostone		6.5	−6.4					
14HA-93	Doushantuo	164.5	Argillaceous limestone		6.1	−3.8					
14HA-91	Doushantuo	160.5	Argillaceous dolostone		6.4	−5.6					
14HA-90	Doushantuo	158.5	Argillaceous dolostone		6.0	−5.8					
14HA-89	Doushantuo	156.5	Calcareous mudstone		6.4	−6.0					
14HA-88	Doushantuo	154.5	Argillaceous limestone		6.5	−6.3					
14HA-87	Doushantuo	153.5	Argillaceous limestone		5.8	−6.6					
14HA-86	Doushantuo	151.5	Calcareous mudstone		6.0	−5.7					
14HA-84	Doushantuo	147.5	Argillaceous limestone		6.4	−9.0					
14HA-83	Doushantuo	145.5	Argillaceous limestone	83.50	5.4	−6.8	0.708439	0.000295	260.86	6476.57	0.04
14HA-82	Doushantuo	143.5	Argillaceous limestone		5.4	−6.8					
14HA-81	Doushantuo	141	Argillaceous limestone		5.7	−7.8					
14HA-80	Doushantuo	138	Argillaceous limestone		6.5	−7.3					
14HA-79	Doushantuo	137	Limestone		6.4	−9.3					
14HA-78	Doushantuo	135	Calcitic dolostone		7.4	−9.7					
14HA-77	Doushantuo	132.8	Limestone		7.5	−9.8					
14HA-76	Doushantuo	131.3	Limestone		7.5	−9.5					
14HA-75	Doushantuo	129.3	Argillaceous limestone		6.3	−10.2					
14HA-74	Doushantuo	127.8	Argillaceous limestone	89.80	6.1	−8.9	0.708555	0.000911	150.32	11915.09	0.01
14HA-73	Doushantuo	124.8	Limestone		6.5	−9.2					
14HA-72	Doushantuo	123.8	Limestone		6.4	−9.6					
14HA-71	Doushantuo	121.8	Limestone		7.1	−8.8					
14HA-70	Doushantuo	119.8	Dolomitic limestone		7.2	−8.5					
14HA-69	Doushantuo	118.8	Dolomitic limestone		7.2	−8.4					
14HA-68	Doushantuo	116.6	Dolomitic limestone		6.7	−10.2					
14HA-67	Doushantuo	114.8	Dolomitic limestone		7.3	−8.7					
14HA-66	Doushantuo	113.2	Calcitic dolostone		6.6	−8.6					
14HA-65	Doushantuo	111.7	Calcitic dolostone		7.0	−7.4					
14HA-64	Doushantuo	110.2	Dolomitic limestone		6.6	−10.3					
14HA-63	Doushantuo	109	Calcitic dolostone		6.7	−9.2					
14HA-62	Doushantuo	106	Dolomitic limestone	79.30	4.7	−12.0	0.708781	0.000720	164.79	8136.74	0.02
14HA-61	Doushantuo	104.5	Dolomitic limestone		5.6	−11.4					
14HA-60	Doushantuo	102.7	Dolomitic limestone		5.5	−9.4					
14HA-59	Doushantuo	100.7	Limestone		5.5	−10.5					
14HA-58	Doushantuo	97.2	Argillaceous limestone		5.6	−10.0					
14HA-57	Doushantuo	95.2	Dolomitic limestone		5.9	−10.4					
14HA-56	Doushantuo	94	Dolomitic limestone		5.9	−10.3					
14HA-54	Doushantuo	92.1	Limestone		6.2	−10.2					
14HA-53	Doushantuo	91.4	Limestone		6.4	−11.0					
14HA-52	Doushantuo	91.2	Limestone		6.6	−11.1					
14HA-51	Doushantuo	90.7	Limestone		6.4	−10.9					
14HA-50	Doushantuo	89.7	Limestone		6.4	−10.8					
14HA-49	Doushantuo	88.2	Limestone	86.40	6.8	−10.4	0.708394	0.001241	120.44	9852.94	0.01
14HA-48	Doushantuo	68.2	Limestone		3.1	−11.3					
14HA-47	Doushantuo	67.7	Limestone	94.70	5.9	−11.9	0.708411	0.001055	119.15	5145.01	0.02
14HA-46	Doushantuo	67.2	Silicified limestone		4.4	−10.6					
14HA-45	Doushantuo	66.9	Calcitic dolostone		4.9	−9.3					
14HA-42	Doushantuo	62.4	Silicified limestone		6.7	−10.9					
14HA-41	Doushantuo	61.3	Calcitic dolostone		6.8	−10.1					
14HA-40	Doushantuo	60.8	Argillaceous dolostone		6.3	−5.3					
14HA-39	Doushantuo	59.8	Calcitic dolostone		5.6	−6.0					
14HA-38	Doushantuo	56.3	Argillaceous dolostone		5.6	−5.4					
14HA-36	Doushantuo	53.1	Argillaceous dolostone	68.70	5.3	−5.1	0.708722	0.000213	615.10	4216.67	0.15
14HA-35	Doushantuo	51.9	Argillaceous dolostone		5.6	−4.7					
14HA-34	Doushantuo	47.9	Argillaceous dolostone		5.2	−3.9					
14HA-33	Doushantuo	46.7	Argillaceous dolostone		5.2	−5.0					
14HA-32	Doushantuo	41.7	Dolostone		2.4	−6.1					
14HA-31	Doushantuo	40.9	Dolostone		2.6	−6.4					
14HA-30	Doushantuo	40	Argillaceous dolostone	50.10	2.9	−10.4	0.710157	0.000443	532.31	5306.55	0.10
14HA-28	Doushantuo	37.4	Argillaceous dolostone		−0.2	−4.1					
14HA-27	Doushantuo	36.2	Argillaceous dolostone		1.7	−6.6					
14HA-25	Doushantuo	24.7	Calcitic dolostone		2.9	−7.0					
14HA-24	Doushantuo	23.7	Argillaceous limestone	72.20	−3.5	−2.8	0.708814	0.001158	977.37	2818.73	0.35
14HA-22	Doushantuo	19.7	Dolostone		4.3	−7.6					
14HA-21	Doushantuo	17.7	Argillaceous dolostone		4.3	−7.5					
14HA-19	Doushantuo	14.7	Argillaceous dolostone		4.2	−8.0					
14HA-18	Doushantuo	13.9	Argillaceous dolostone		4.4	−7.3					

(*continued on next page*)

Table 2 (*continued*)

Sample	Formation	Height (m)*	Lithology	Carbonate content (%)	$\delta^{13}C_{PDB}$	$\delta^{18}O_{PDB}$	$^{87}Sr/^{87}Sr$	$^{87}Rb/^{87}Sr$	Mn (ppm)	Sr (ppm)	Mn/Sr
14HA-17	Doushantuo	12.7	Argillaceous dolostone		3.6	−7.2					
14HA-16	Doushantuo	12	Argillaceous dolostone		4.0	−9.7					
14HA-15	Doushantuo	11.5	Argillaceous dolostone		3.0	−7.6					
14HA-14	Doushantuo	11	Dolostone		3.6	−9.9					
14HA-13	Doushantuo	10	Dolostone		3.9	−9.8					
14HA-12	Doushantuo	8	Calcareous mudstone		2.3	−3.9					
14HA-11	Doushantuo	5	Dolostone	51.80	3.4	−4.8	0.708364	0.000546	3680.05	4919.22	0.75
14HA-10	Doushantuo	4.2	Argillaceous limestone		2.8	−4.9					
14HA-9	Doushantuo	3.4	Silty limestone		2.1	−3.9					
14HA-8	Doushantuo	2.5	Dolomitic limestone	54.90	−4.6	−7.4	0.712234	0.000283	13273.47	2591.25	5.12
14HA-7	Doushantuo	2.05	Dolostone		−1.7	−8.7					
14HA-6	Doushantuo	1.85	Dolostone		−1.8	−8.0					
14HA-5	Doushantuo	1.65	Dolostone		−3.5	−10.4					
14HA-4	Doushantuo	1.6	Dolostone		−4.1	−9.9					
14HA-3	Doushantuo	1.1	Dolostone	44.90	−3.1	−10.2	0.716621	0.000760	26821.72	1805.05	14.86
14HA-2	Doushantuo	0.6	Dolostone		−4.3	−8.9					
14HA-1	Doushantuo	0	Dolostone		−3.0	−7.2					

* Stratigraphic height is measured from the base of the Doushantuo Formation.

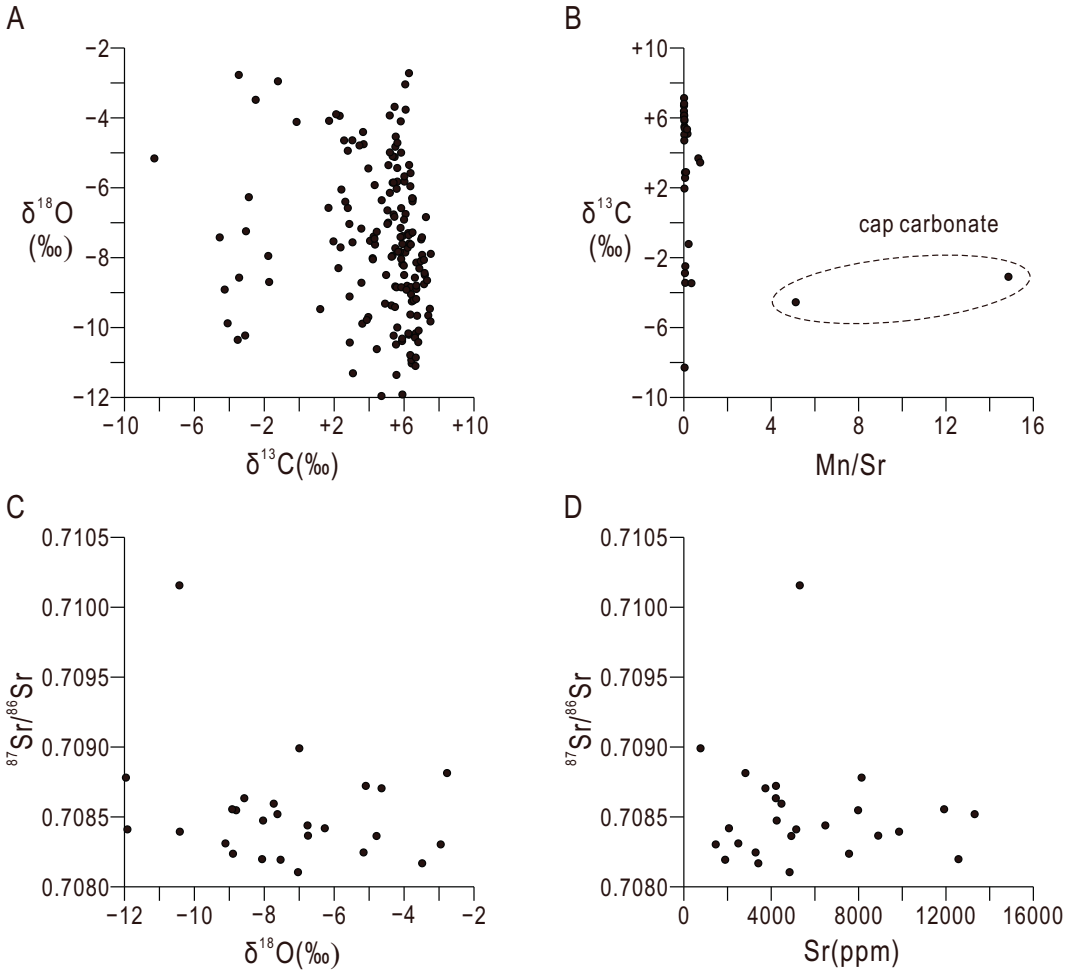

Fig. 10. Cross plots of isotope and elemental data of the Doushantuo Formation at the Lujiayuanzi section.

$\delta^{13}C$ and $\delta^{18}O$ values (Fig. 10A, Table 2). With the exception of two samples from the cap carbonate, all samples have Mn/Sr ratios less than 1.00, and many have ratios lower than 0.10 (Fig. 10B, Table 2), suggesting little diagenetic overprinting of $\delta^{13}C$ (Kaufman and Knoll, 1995).

$^{87}Sr/^{86}Sr$ values above the cap carbonate at Lujiayuanzi are randomly scattered between 0.7081 and 0.7101, and fluctuate around 0.7085 throughout the Doushantuo Formation, exhibiting no consistent stratigraphic trends (Fig. 3; Table 2). They are significantly more radiogenic than previously published data from the

Doushantuo Formation in South China (Cui et al., 2015; Sawaki et al., 2010) and lower–middle Ediacaran successions around the world (Halverson et al., 2007; Narbonne et al., 2012; Xiao et al., 2016). $^{87}Sr/^{86}Sr$ and $\delta^{18}O$ values do not show positive correlation, and Sr concentrations for the studied Doushantuo samples are generally higher than 2000 ppm, with a mean value of 5220 ppm (Fig. 10C, D, Table 2). Thus, the elevated $^{87}Sr/^{86}Sr$ ratios of the Doushantuo Formation at the Lujiayuanzi section, relative to other age-equivalent strata, are enigmatic. It is possible that the high $^{87}Sr/^{86}Sr$ ratios may be attributed to the dissolution of recrystallized calcite and clay minerals during acid leaching in the laboratory (e.g. Liu et al., 2013b).

5. Discussion

5.1. Regional and global comparisons of DPA composition at Lujiayuanzi section

Most (seven in eight) acanthomorph species identified from the Lujiayuanzi section have been previously known from the Doushantuo Formation in the Yangtze Gorges area of South China (Table 3). However, the two taxonomically distinct and biostratigraphically significant DPA assemblage zones established in the Yangtze Gorges area cannot be distinguished at Lujiayuanzi (Liu et al., 2013a, 2014a,b; McFadden et al., 2009; Yin et al., 2011a; Zhou et al., 2007). The eponymous taxa of the two assemblage zones, *Tianzhushania spinosa* and *Hocosphaeridium anozos*, have not been recovered from the Lujiayuanzi section. It should be emphasized, however, that the lowest DPA-bearing bed at Lujiayuanzi is only ~40 m above the base of the Doushantuo Formation and occurs in the lower shallowing upward sequence (Fig. 3). Lithostratigraphic correlation with the Doushantuo Formation in the Yangtze Gorges area suggests that acanthomorphic acritarchs discovered at horizons of ~40 m and 114.8 m at the Lujiayuanzi section may be assigned to *Tianzhushania spinosa* assemblage zone (Fig. 11). Among the eight taxonomically identified acanthomorph species found at Lujiayuanzi, ?*Cavaspina basiconica*, *Knollisphaeridium maximum*, and *Mengeosphaera chadianensis* are known to occur in both the *Tianzhushania spinosa* and *Hocosphaeridium anozos* assemblage zones in the Yangtze Gorges area (Table 3), whereas among the other five species, *Mengeosphaera*? *cuspidata*, *M. latibasis*?, *M. spicata*?, and *Urasphaera fungiformis* were erected by Liu et al. (2014b) based on specimens found in the *Hocosphaeridium anozos* assemblage zone in the Yangtze Gorges area. Additionally, leiosphere clusters at two horizons near 213 m in the Lujiayuanzi section resemble those characterize in the *Hocosphaeridium anozos* assemblage zone in the Yangtze Gorges area (Liu et al., 2014b; Yin et al., 2011a). Thus, although the limited number of taxa at Lujiayuanzi does not allow a recognition of the two DPA assemblage zones established in the Yangtze Gorges, elements of the *Hocosphaeridium anozos* assemblage zone are also recorded at Lujiayuanzi.

Attempts to identify the *Tianzhushania spinosa* and *Hocosphaeridium anozos* assemblage zones outside South China have yielded limited success. Elements of the *Tianzhushania spinosa* assemblage zone, including the eponymous species, have been identified from the Infrakrol Formation in the Lesser Himalaya region of northern India (Joshi and Tiwari, 2016), establishing a possible biostratigraphic tie point between South China and northern India. Similarly, many elements of the *Hocosphaeridium anozos* assemblage zone, including the eponymous species, have been found in the Ediacaran complex acanthomorphic palynoflora (ECAP) of Australia (Grey, 2005; Willman and Moczydłowska, 2008). Ediacaran acanthomorph assemblages from Siberia and East European Platform are taxonomically diverse, but thus far neither

Table 3
A list of DPA genera and species from the Doushantuo Formation at Lujiayuanzi and their global occurrence.

		Genus *Appendisphaera*	*Appendisphaera fragilis*	Genus *Cavaspina*	?*Cavaspina basiconica*	Genus *Knollisphaeridium*	*Knollisphaeridium maximum*	Genus *Mengeosphaera*	*Mengeosphaera chadianensis*	*M.? cuspidata*	*M. latibasis?*	*M. spicata?*	Genus *Urasphaera*	*Urasphaera fungiformis*
Lujiyuanzi		•												
Yangtze Gorges area	*Tianzhushania spinosa* assemblage zone	•	•	•	•	•	•	•	•	•	•	•	•	•
	Hocosphaeridium anozos assemblage zone	•		•	•	•	•	•	•	•	•	•	•	•
Weng'an		•	•	•	•	•	•	•	•					
Australia		•	•	•	•	•	•						•	
Siberia		•	•	•	•	•	•							
East European Platform		•	•	•		•	•							
Lesser Himalaya			•											
Svalbard														
Southern Norway		•						•						

* Denotes presence of the genus/species. Data sources: Yangtze Gorges area (Liu et al., 2013a, 2014b; McFadden et al., 2009; Yin et al., 2007; Zhang et al., 1998); Weng'an (Xiao et al., 2014; Yin et al., 2011b); Australia (Grey, 2005); Siberia (Moczydłowska, 2005; Moczydłowska and Nagovitsin, 2012); Lesser Himalaya (Shukla and Tiwari, 2014; Tiwari and Knoll, 1994; Tiwari and Pant, 2004); Svalbard (Knoll, 1992); Southern Norway (Adamson and Butterfield, 2014).

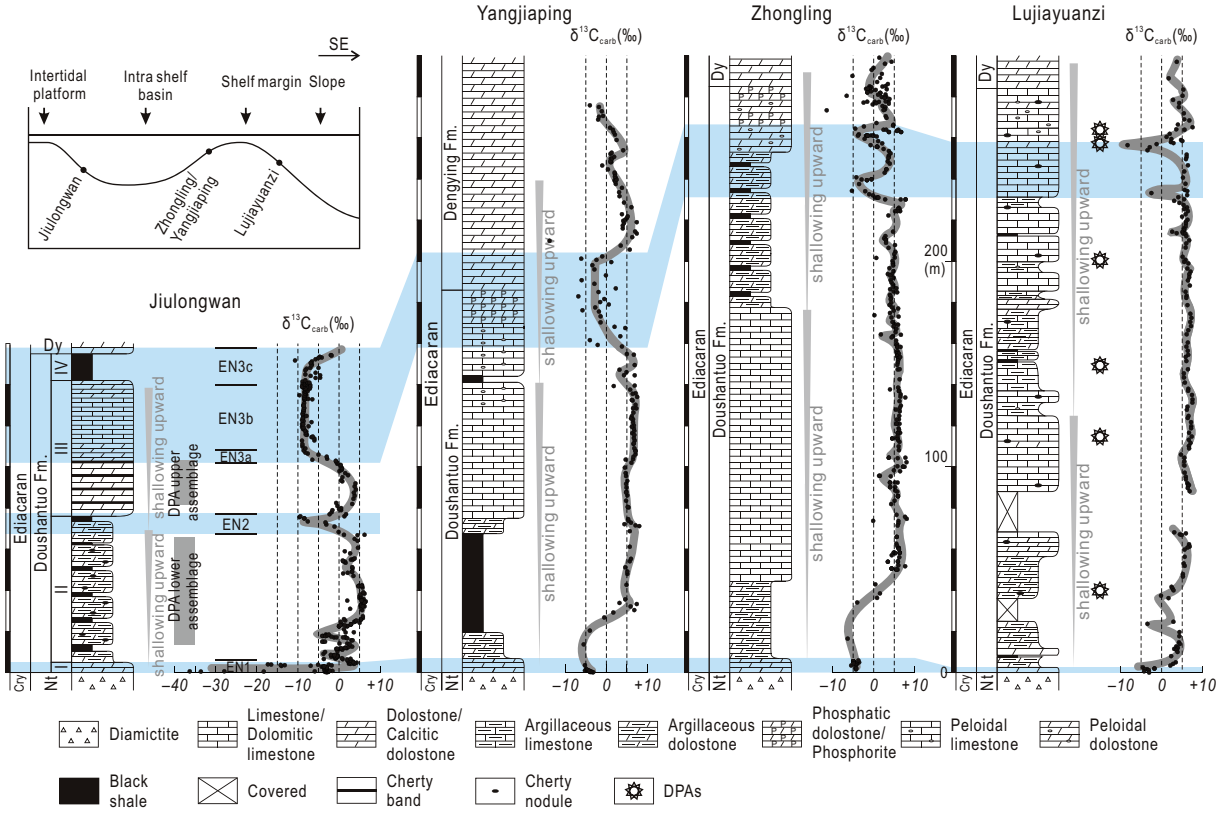

Fig. 11. Litho- and chemostratigraphic correlations of the Doushantuo Formation in the shelf basin (Jiulongwan section), the outer shelf (Zhongling and Yangjiaping sections), and the upper slope (Lujiayuanzi section). Data sources: Jiulongwan section, McFadden et al. (2008); Yangjiaping section, Cui et al. (2015) and Kunimitsu et al. (2011); Zhongling section, Cui et al. (2015, 2017) and Zhu et al. (2007); Lujiayuanzi section, this study. Fossils data for the Jiulongwan section are from Liu et al. (2014a) and Zhou et al. (2007). DPAs: Doushantuo-Pertataka acritarchs. Cry: Cryogenian. Nt: Nantuo Formation. Dy: Dengying Formation.

Tianzhushania spinosa nor *Hocosphaeridium anozos* have been found (Xiao et al., 2014).

5.2. Biostratigraphic implications of DPAs in the Lujiyuanzi section

5.2.1. Stratigraphic correlation of the Doushantuo Formation between the Lujiayuanzi section and the Yangtze Gorges area

In the Yangtze block, Ediacaran successions consist of the Doushantuo and Dengying formations or their equivalents. The lower and middle Ediacaran (~635–551 Ma) Doushantuo Formation is dominated by organic-rich siliciclastics and carbonate rocks, whereas upper Ediacaran strata consist of Dengying Formation dolostone deposited in shallow water facies and Liuchapo Formation siliceous rocks deposited in slope and basinal facies (Cao et al., 1989). While the thickness and lithology vary in different depositional facies, the Doushantuo Formation in slope/basinal facies (e.g., the Siduping section in Hunan Province and the Wuhe section in Guizhou Province, as well as the Lantian Formation in southern Anhui Province) can be easily correlated with the Doushantuo Formation in the Yangtze Gorges area (i.e., Jiulongwan section) (Jiang et al., 2007; Wang et al., 2016, 2017a; Yuan et al., 2011). This correlation is further supported by numerous C and Sr isotope chemostratigraphic studies (Jiang et al., 2007; Lu et al., 2013; Wang et al., 2016; Zhou and Xiao, 2007; Zhu et al., 2007, 2013).

Since Sr isotopic data in the Lujiayuanzi section fail to serve as a stratigraphic correlation tool as discussed above, the attempt to correlate the Doushantuo Formation at Lujiayuanzi and other localities is mainly based on lithostratigraphic sequence and carbon isotopic profiles.

The Doushantuo Formation at Lujiayuanzi and Zhongling (also in the northwestern Hunan Province), both of which were deposited in the marginal shelf environment, can be readily correlated (Figs. 2 and 11). Several chemostratigraphic studies have been carried out at the Zhongling section and the nearby Yangjiaping section (Cui et al., 2015; Furuyama et al., 2016; Kunimitsu et al., 2011; Li et al., 2010; Zhu et al., 2007). At both Lujiayuanzi and Zhongling sections, the Doushantuo Formation can be subdivided into two shallowing-upward sequences: the lower sequence is shale-dominated at the bottom part and is followed by a pure limestone interval, whereas the upper sequence starts with carbonate rocks intercalated with argillaceous carbonate or shale, which is succeeded by tens of meters intraclastic carbonate rocks and phosphorite beds (Fig. 11).

Carbon isotopic profile of the Doushantuo Formation at Lujiayuanzi also resembles that of the shelf margin Zhongling section (Fig. 11). At both sections, the cap carbonate yields negative values and can be correlated with EN1 in the Yangtze Gorges area. The lower few to tens of meters of strata above the cap carbonate are characterized by frequent variations in $\delta^{13}C_{carb}$ values around 0‰, a feature that has also been reported from equivalent strata at other sections across the Yangtze Block (Wang et al., 2017b). Above that, $\delta^{13}C_{carb}$ values remain quite constant at ~+5‰ for most part of Doushantuo Formation at Zhongling and Lujiayuanzi until in the uppermost part where $\delta^{13}C_{carb}$ values show pronounced fluctuations, with the lowest value reaching −8.3‰ at the Lujiayuanzi section (Figs. 3, 11).

The Doushantuo Formation at the Zhongling and Yangjiaping sections was traditionally correlated with the entire Doushantuo Formation at Jiulongwan in the Yangtze Gorges area, with the C

isotopic excursion in the upper Doushantuo Formation at Zhongling and Yangjiaping correlated with EN3 at Jiulongwan (Li et al., 2010; Zhu et al., 2007). Mainly based on $^{87}Sr/^{86}Sr$ ratios which rise at the onset of the upper Doushantuo C isotopic excursion and reach a peak of 0.7085 at Yangjiaping and 0.7083 at Zhongling, Cui et al. (2015) re-evaluated this correlation and considered the upper Doushantuo C isotopic excursion of the outer shelf sections as equivalent to the lower part of EN3, i.e., EN3a recognized by McFadden et al. (2008). Accordingly, the main part of EN3 (EN3b in thin-bedded limestone + EN3c in the carbonate concretions within black shales, McFadden et al., 2008), in which the $^{87}Sr/^{86}Sr$ ratio reaches 0.7090 in Yangtze Gorges area (Sawaki et al., 2010), is missing from the Zhongling section (Cui et al., 2015). This interpretation predicts a depositional break in the uppermost Doushantuo Formation at Zhongling and Yangjiaping sections. However, no obvious stratigraphic break or subaerial erosion has been observed at these sections, although the existence of cryptic sedimentary breaks cannot be ruled out, considering that the prevalent occurrence of oolitic and intraclastic carbonates in the uppermost Doushantuo Formation at Zhongling and Yangjiaping suggests deposition in an overall shallow and high-energy intertidal environment (Vernhet and Reijmer, 2010). Alternatively, the main part of EN3 may extend to the lower Dengying Formation at Zhongling and Yangjiaping sections, implying the diachronous nature of the Doushantuo/Dengying boundary (Cui et al., 2015). Detailed $\delta^{13}C$ investigation of multiple sections of the Doushantuo Formation in the Yangtze Gorges area indicates that the presence of EN3b is dependent on the occurrence of thin-bedded limestone, whose absence in many sections may be due to rapid lateral facies change and/or cryptic sedimentary breaks (Zhou et al., 2017).

Furuyama et al. (2016) recently proposed that the negative C isotopic excursion in the upper Doushantuo Formation at Yangjiaping can be alternatively correlated with EN2 in the Yangtze Gorges area. The elevated $^{87}Sr/^{86}Sr$ ratios up to 0.7085 in the upper Doushantuo Formation at Yangjiaping were used to support a correlation with the middle Doushantuo Formation in the Yangtze Gorges area, which hosts EN2 and features similarly elevated $^{87}Sr/^{86}Sr$ ratios (Sawaki et al., 2010). Accordingly, Furuyama et al. (2016) inferred that strata equivalent to Member III and IV in the Yangtze Gorges area are completely missing from the Yangjiaping section. However, the elevated $^{87}Sr/^{86}Sr$ ratios at the EN2 interval in the Yangtze Gorges area are mostly from dolomitic and argillaceous samples (Sawaki et al., 2010), which are unsuitable for Sr isotopic measurements (Cui et al., 2015; Xiao et al., 2016). Additionally, this rise in $^{87}Sr/^{86}Sr$ below EN3 has not been reported from synchronous Doushantuo limestones outside the Yangtze Gorges area. More importantly, this correlation is inconsistent with lithostratigraphic sequences of the Doushantuo Formation, which demonstrates two shallowing-up cycles at both localities (Fig. 11) (Jiang et al., 2011).

In summary, the similar lithostratigraphic sequences of the Doushantuo Formation in shelf basin and shelf margin environments support the correlation of the upper Doushantuo C isotopic excursions between the shelf margin sections (e.g., Lujiayuanzi, Zhongling, and Yangjiaping) and the shelf basin sections (e.g., Jiulongwan in the Yangtze Gorges area). Our preferred correlation suggests that the negative carbon isotope excursion in the upper Doushantuo Formation at Lujiayuanzi, Yangjiaping, and Zhongling section can be approximately correlated with EN3 at the Jiulongwan section (Fig. 11).

5.2.2. Relationship between DPA's stratigraphic range and EN3

Previously, occurrences of DPAs have only been confirmed from stratigraphic horizons below EN3 or their equivalent intervals (Golubkova et al., 2010; Grey, 2005; Grey and Calver, 2007; Liu et al., 2014a; Lu et al., 2013; McFadden et al., 2008; Zhou et al., 2007). It has been further speculated that environmental changes (e.g., surface water anoxia, final oxidation of the global ocean) as recorded in EN3 drove the extinction of DPAs (Cohen et al., 2009; Jiang et al., 2007; Zhou et al., 2012). However, the preservation of DPAs is strongly influenced by taphonomic processes and the full stratigraphic range of DPAs may have been underestimated. For example, in the Yangtze Block, DPAs are only preserved in early diagenetic chert nodules and phosphorites, which are rare above EN3. Similarly, in Australia where DPAs are preserved as organic-walled microfossils in fine grained siliciclastic rocks, Ediacaran succession above the Wonoka excursion is dominated by sandstone (Grey, 2005; Grey and Calver, 2007). Thus, the disappearance of DPAs after EN3/Wonoka excursion may also be due to the absence of lithologies suitable for DPA preservation.

The uppermost two DPA-containing beds in the Lujiayuanzi section (i.e., *Knollisphaeridium* and *Mengeosphaera* at 264 m, a poorly-preserved acanthomorph at 257.5 m, respectively) are both above the $\delta^{13}C$ negative excursion. If we accept the correlation between the upper Doushantuo C isotopic anomaly at the Lujiayuanzi section and EN3 in the Yangtze Gorges area, the occurrence of *Knollisphaeridium* and *Mengeosphaera* at Lujiayuanzi suggests that some elements of large acanthomorphic acritarchs may have survived whatever environmental change recorded by EN3, opening the possibility that DPAs may co-occur with Ediacara-type macroscopic organisms.

The stratigraphic relationship between DPAs and Ediaraca-type macrofossils has been a matter of debate. Knoll and Walter (1992) proposed that DPAs largely predate Ediacara-type macrofossils, and the observation that the Ediacara-type macrofossils appeared immediately after the Gaskiers glaciation indicates that DPAs and Ediacara-type macrofossils may be separated by the ~580 Ma Gaskiers glaciation (Xiao and Laflamme, 2009). However, largely owing to the absence of reliable radiometric ages for the Ediacaran carbon isotopic excursions, the Gaskiers glaciation has been variously correlated with the WANCE negative carbon isotope excursion in the lower Doushantuo Formation (Condon et al., 2005; Zhu et al., 2013), the positive carbon isotope excursion EP1 in the lower Doushantuo Formation based on the occurrence of glendonites (Wang et al., 2017b), the negative carbon isotopic excursion EN2 in the middle Doushantuo Formation (Macdonald et al., 2013; Sawaki et al., 2010), or the negative carbon isotope excursion EN3 in the uppermost Doushantuo Formation (Halverson et al., 2005; Wang et al., 2014; Xiao, 2004a; Zhou et al., 2007). These divergent correlations make it difficult to resolve the stratigraphic relationship between DPAs and Ediacara-type macrofossils, thus complicating our efforts to sequence Ediacaran evolutionary, climatic, and geochemical events (Xiao et al., 2016). However, there are increasing evidence suggesting that elements of the Ediacara biota may range downward to the lower Ediacaran System (Macdonald et al., 2013; Xiao et al., 2013) and some DPA taxa may range upward above the level of Shuram excursion (Golubkova et al., 2015; this study). DPAs and Ediacara-type macrofossils may have overlapping stratigraphic ranges, regardless how the carbon isotope excursions are correlated with Gaskiers glaciation.

6. Conclusions

The Doushantuo Formation at the Lujiayuanzi section is mainly composed of carbonate rocks that were deposited in an upper slope environment. Five genera and eight species of Doushantuo-Pertatataka acritarchs (DPAs), together with a few other silicified microfossils, have been recovered from chert nodule horizons throughout the Doushantuo Formation at Lujiayuanzi. DPA taxa at Lujiayuanzi are taxonomically similar to those from the

Doushantuo Formation in the Yangtze Gorges area. The lower and upper assemblage zones identified in the Doushantuo Formation in the Yangtze Gorges area, however, have not been recognized at Lujiayuanzi.

At Lujiayuanzi, the highest DPA-bearing beds are above a $\delta^{13}C$ negative excursion that can be correlated with EN3 in in the upper Doushantuo Formation, which has been correlated with the Shuram negative carbon isotope excursion. Thus, the last appearance of DPAs in the Lujiayuanzi section may postdate the EN3/Shuram/Wonoka excursion, suggesting that DPAs may have survived the environmental perturbation represented by EN3 and co-existed with the Ediacara-type macroscopic organisms in the late Ediacaran Period. More palaeontological investigation is needed to test this expectation.

Acknowledgments

This work was supported by the Strategic Priority Research Program (B) of Chinese Academy of Sciences (grant number XDB18000000), the National Natural Science Foundation of China (grant number 41672027), National Basic Research Program of China (grant number 2013CB835005), and the US National Science Foundation (EAR1528553). We are grateful to three anonymous reviewers for their constructive comments and suggestions.

References

Adamson, P.W., Butterfield, N.J., 2014. Palaeobiology of a Doushantuo-type acanthomorphic acritarch assemblage from the Ediacaran Biskopås Formation, Southern Norway. In: Abstracts of South China 2014: A symposium and field workshop on Ediacaran and Cryogenian Stratigraphy, pp. 1–2.

An, Z., Jiang, G., Tong, J., Tian, L., Ye, Q., Song, H., Song, H., 2015. Stratigraphic position of the Ediacaran Miaohe biota and its constrains on the age of the upper Doushantuo $\delta^{13}C$ anomaly in the Yangtze Gorges area, South China. Precambr. Res. 271, 243–253.

Cao, R., Tang, T., Xue, Y., Yu, C., Yin, L., Zhao, W., 1989. Research on Sinian Strata with ore deposits in the Yangzi (Yangtze) Region, China. In: Nanjing Institute of Geology and Palaeontology, Chinese Academy of Sciences (Ed.), Upper Precambrian of the Yangzi (Yangtze) Region. Nanjing University Press, China, pp. 1–94.

Chen, L., Xiao, S., Pang, K., Zhou, C., Yuan, X., 2014. Cell differentiation and germ-soma separation in Ediacaran animal embryo-like fossils. Nature 516, 238–241.

Cohen, P.A., Knoll, A.H., Kodner, R.B., 2009. Large spinose microfossils in Ediacaran rocks as resting stages of early animals. Proc. Natl. Acad. Sci. U.S.A. 106 (16), 6519–6524.

Condon, D., Zhu, M., Bowring, S., Wang, W., Yang, A., Jin, Y., 2005. U-Pb ages from the Neoproterozoic Doushantuo Formation, China. Science 308 (5718), 95–98.

Cui, H., Kaufman, A.J., Xiao, S., Zhou, C., Liu, X., 2017. Was the Ediacaran Shuram Excursion a globally synchronized early diagenetic event? Insights from methane-derived authigenic carbonates in the uppermost Doushantuo Formation, South China. Chem. Geol. 450, 59–80.

Cui, H., Kaufman, A.J., Xiao, S., Zhu, M., Zhou, C., Liu, X.-M., 2015. Redox architecture of an Ediacaran ocean margin: integrated chemostratigraphic ($\delta^{13}C$–$\delta^{34}S$–$^{87}Sr/^{86}Sr$–Ce/Ce*) correlation of the Doushantuo Formation, South China. Chem. Geol. 405, 48–62.

Furuyama, S., Kano, A., Kunimitsu, Y., Ishikawa, T., Wang, W., 2016. Diagenetic overprint to a negative carbon isotope anomaly associated with the Gaskiers glaciation of the Ediacaran Doushantuo Formation in South China. Precambr. Res. 276, 110–122.

Golubkova, E.Y., Raevskaya, E.G., Kuznetsov, A.B., 2010. Lower Vendian microfossil assemblages of East Siberia: significance for solving regional stratigraphic problems. Stratigr. Geol. Correl. 18 (4), 353–375.

Golubkova, E.Y., Zaitseva, T.S., Kuznetsov, A.B., Dovzhikova, E.G., Maslov, A.V., 2015. Microfossils and Rb-Sr age of glauconite in the key section of the Upper Proterozoic of the northeastern part of the Russian plate (Keltmen-1 borehole). Dokl. Earth Sci. 462 (2), 547–551.

Grey, K., 2005. Ediacaran palynology of Australia. Mem. Assoc. Australas. Palaeontol. 31, 1–439.

Grey, K., Calver, C.R., 2007. Correlating the Ediacaran of Australia. Geol. Soc. London Specl. Publ. 286 (1), 115–135.

Grey, K., Walter, M.R., Calver, C.R., 2003. Neoproterozoic biotic diversification: Snowball Earth or aftermath of the Acraman impact? Geology 31 (5), 459–462.

Grotzinger, J.P., Fike, D.A., Fischer, W.W., 2011. Enigmatic origin of the largestknown carbon isotope excursion in Earth's history. Nat. Geosci. 4 (5), 285–292.

Halverson, G.P., Dudás, F.Ö., Maloof, A.C., Bowring, S.A., 2007. Evolution of the $^{87}Sr/^{86}Sr$ composition of Neoproterozoic seawater. Palaeogeogr. Palaeoclimatol. Palaeoecol. 256 (3–4), 103–129.

Halverson, G.P., Hoffman, P.F., Schrag, D.P., Maloof, A.C., Rice, A.H.N., 2005. Toward a Neoproterozoic composite carbon-isotope record. Geol. Soc. Am. Bull. 117 (9–10), 1181–1207.

Hawkins, A., Xiao, S., Jiang, G., Shi, X., Wang, X., 2014. Acritarch biostratigraphy of the Ediacaran Doushantuo Formation in an upper slope facies, 2014 GSA Annual Meeting. Vancouver, British Columbia.

Jiang, G., Kaufman, A.J., Christie-Blick, N., Zhang, S., Wu, H., 2007. Carbon isotope variability across the Ediacaran Yangtze platform in South China: implications for a large surface-to-deep ocean $\delta^{13}C$ gradient. Earth Planet. Sci. Lett. 261 (1–2), 303–320.

Jiang, G., Shi, X., Zhang, S., Wang, Y., Xiao, S., 2011. Stratigraphy and paleogeography of the Ediacaran Doushantuo Formation (ca. 635–551 Ma) in South China. Gondwana Res. 19 (4), 831–849.

Jiang, G., Sohl, L.E., Christie-Blick, N., 2003. Neoproterozoic stratigraphic comparison of the Lesser Himalaya (India) and Yangtze block (South China): paleogeographic implications. Geology 31 (10), 917–920.

Joshi, H., Tiwari, M., 2016. *Tianzhushania spinosa* and other large acanthomorphic acritarchs of Ediacaran Period from the Infrakrol Formation, Lesser Himalaya, India. Precambr. Res. 286, 325–336.

Kaufman, A.J., Knoll, A.H., 1995. Neoproterozoic variations in the C-isotopic composition of seawater: stratigraphic and biogeochemical implications. Precambr. Res. 73 (1–4), 27–49.

Knoll, A.H., 1992. Vendian microfossils in metasedimentary cherts of the Scotia group, Prins Karls Forland, Svalbard. Palaeontology 35 (4), 751–774.

Knoll, A.H., Walter, M.R., 1992. Latest Proterozoic stratigraphy and earth history. Nature 356 (6371), 673–677.

Kunimitsu, Y., Setsuda, Y., Furuyama, S., Wang, W., Kano, A., 2011. Ediacaran chemostratigraphy and paleoceanography at a shallow marine setting in northwestern Hunan Province, South China. Precambr. Res. 191 (3–4), 194–208.

Li, C., Love, G.D., Lyons, T.W., Fike, D.A., Sessions, A.L., Chu, X., 2010. A stratified redox model for the Ediacaran Ocean. Science 328, 80–83.

Li, D., Shields-Zhou, G.A., Ling, H.-F., Thirlwall, M., 2011. Dissolution methods for strontium isotope stratigraphy: guidelines for the use of bulk carbonate and phosphorite rocks. Chem. Geol. 290 (3–4), 133–144.

Li, Z.-X., Zhang, L., Powell, C.M., 1995. South China in Rodinia: part of the missing link between Australia-East Antarctica and Laurentia? Geology 23 (5), 407–410.

Liu, C., Wang, Z., Raub, T.D., 2013b. Geochemical constraints on the origin of Marinoan cap dolostones from Nuccaleena Formation, South Australia. Chem. Geol. 351, 95–104.

Liu, P., Chen, S., Zhu, M., Li, M., Yin, C., Shang, X., 2014a. High-resolution biostratigraphic and chemostratigraphic data from the Chenjiayuanzi section of the Doushantuo Formation in the Yangtze Gorges area, South China: implication for subdivision and global correlation of the Ediacaran System. Precambr. Res. 249, 199–214.

Liu, P., Xiao, S., Yin, C., Chen, S., Zhou, C., Li, M., 2014b. Ediacaran acanthomorphic acritarchs and other microfossils from chert nodules of the upper Doushantuo Formation in the Yangtze Gorges Area, South China. J. Paleontol. Mem. 88 (Suppl. 72), 1–139.

Liu, P., Yin, C., Chen, S., Tang, F., Gao, L., 2013a. The biostratigraphic succession of acanthomorphic acritarchs of the Ediacaran Doushantuo Formation in the Yangtze Gorges area, South China and its biostratigraphic correlation with Australia. Precambr. Res. 225, 29–43.

Lu, M., Zhu, M., Zhang, J., Shields-Zhou, G., Li, G., Zhao, F., Zhao, X., Zhao, M., 2013. The DOUNCE event at the top of the Ediacaran Doushantuo Formation, South China: broad stratigraphic occurrence and non-diagenetic origin. Precambr. Res. 225, 86–109.

Macdonald, F.A., Strauss, J.V., Sperling, E.A., Halverson, G.P., Narbonne, G.M., Johnston, D.T., Kunzmann, M., Schrag, D.P., Higgins, J.A., 2013. The stratigraphic relationship between the Shuram carbon isotope excursion, the oxygenation of Neoproterozoic oceans, and the first appearance of the Ediacara biota and bilaterian trace fossils in northwestern Canada. Chem. Geol. 362, 250–272.

Macouin, M., Besse, J., Ader, M., Gilder, S., Yang, Z., Sun, Z., Agrinier, P., 2004. Combined paleomagnetic and isotopic data from the Doushantuo carbonates, South China: implications for the "snowball Earth" hypothesis. Earth Planet. Sci. Lett. 224 (3–4), 387–398.

McFadden, K.A., Huang, J., Chu, X., Jiang, G., Kaufman, A.J., Zhou, C., Yuan, X., Xiao, S., 2008. Pulsed oxidation and biological evolution in the Ediacaran Doushantuo Formation. Proc. Natl. Acad. Sci. U.S.A. 105 (9), 3197–3202.

McFadden, K.A., Xiao, S., Zhou, C., Kowalewski, M., 2009. Quantitative evaluation of the biostratigraphic distribution of acanthomorphic acritarchs in the Ediacaran Doushantuo Formation in the Yangtze Gorges area, South China. Precambr. Res. 173, 170–190.

Moczydłowska, M., 2005. Taxonomic review of some Ediacaran acritarchs from the Siberian Platform. Precambr. Res. 136 (3–4), 283–307.

Moczydłowska, M., 2015. Algal affinities of Ediacaran and Cambrian organic-walled microfossils with internal reproductive bodies: Tanarium and other morphotypes. Palynology 40 (1), 83–121.

Moczydłowska, M., Nagovitsin, K.E., 2012. Ediacaran radiation of organic-walled microbiota recorded in the Ura Formation, Patom Uplift, East Siberia. Precambr. Res. 198–199, 1–24.

Narbonne, G.M., Xiao, S., Shields, G.A., Gehling, J.G., 2012. Chapter 18 – The Ediacaran Period. In: Gradstein, F.M., Ogg, J.G., Schmitz, M.D., Ogg, G.M. (Eds.), The Geologic Time Scale. Elsevier, Boston, pp. 413–435.

Sawaki, Y., Ohno, T., Tahata, M., Komiya, T., Hirata, T., Maruyama, S., Windley, B.F., Han, J., Shu, D., Li, Y., 2010. The Ediacaran radiogenic Sr isotope excursion in the

Doushantuo Formation in the Three Gorges area, South China. Precambr. Res. 176 (1–4), 46–64.
Shukla, R., Tiwari, M., 2014. Ediacaran acanthomorphic acritarchs from the Outer Krol Belt, Lesser Himalaya, India: their significance for global correlation. Palaeoworld 23 (3–4), 209–224.
Tiwari, M., Knoll, A.H., 1994. Large acanthomorphic acritarchs from the Infrakrol Formation of the Lesser Himalaya and their stratigraphic significance. J. Himalayan Geol. 5 (2), 193–201.
Tiwari, M., Pant, C.C., 2004. Neoproterozoic silicified microfossils in Infra krol Formation, Lesser Himalaya, India. Himalayan Geol. 25 (1), 1–21.
Vernhet, E., Reijmer, J.J.G., 2010. Sedimentary evolution of the Ediacaran Yangtze platform shelf (Hubei and Hunan provinces, Central China). Sed. Geol. 225 (3–4), 99–115.
Wang, W., Guan, C., Zhou, C., Peng, Y., Pratt, L.M., Chen, X., Chen, L., Chen, Z., Yuan, X., Xiao, S., 2017a. Integrated carbon, sulfur, and nitrogen isotope chemostratigraphy of the Ediacaran Lantian Formation in South China: Spatial gradient, ocean redox oscillation, and fossil distribution. Geobiology 15, 552–571.
Wang, W., Zhou, C., Guan, C., Yuan, X., Chen, Z., Wan, B., 2014. An integrated carbon, oxygen, and strontium isotopic studies of the Lantian Formation in South China with implications for the Shuram anomaly. Chem. Geol. 373, 10–26.
Wang, X., Jiang, G., Shi, X., Xiao, S., 2016. Paired carbonate and organic carbon isotope variations of the Ediacaran Doushantuo Formation from an upper slope section at Siduping, South China. Precambr. Res. 273, 53–66.
Wang, Z., Wang, J., Suess, E., Wang, G., Chen, C., Xiao, S., 2017b. Silicified glendonites in the Ediacaran Doushantuo Formation (South China) and their potential paleoclimatic implications. Geology 45 (2), 115–118.
Willman, S., Moczydłowska, M., 2008. Ediacaran acritarch biota from the Giles 1 drillhole, Officer Basin, Australia, and its potential for biostratigraphic correlation. Precambr. Res. 162 (3), 498–530.
Xiao, S., 2004a. Neoproterozoic glaciations and the fossil record. In: Jenkins, G.S., McMenamin, M.A.S., McKay, C.P., Sohl, L. (Eds.), The Extreme Proterozoic: Geology, Geochemistry, and Climate. American Geophysical Union, Washington DC, pp. 199–214.
Xiao, S., 2004b. New multicellular algal fossils and acritarchs in Doushantuo chert nodules (Newproterozoic; Yangtze Gorges, South China). J. Paleontol. 78 (2), 393–401.
Xiao, S., Droser, M., Gehling, J.G., Hughes, I.V., Wan, B., Chen, Z., Yuan, X., 2013. Affirming life aquatic for the Ediacara biota in China and Australia. Geology 41 (10), 1095–1098.
Xiao, S., Knoll, A.H., Yuan, X., Pueschel, C.M., 2004. Phosphatized multicellular algae in the Neoproterozoic Doushantuo Formation, China, and the early evolution of florideophyte red algae. Am. J. Bot. 91 (2), 214–227.
Xiao, S., Laflamme, M., 2009. On the eve of animal radiation: phylogeny, ecology and evolution of the Ediacara biota. Trends Ecol. Evol. 24 (1), 31–40.
Xiao, S., Narbonne, G.M., Zhou, C., Laflamme, M., Grazhdankin, D.V., Moczydlowska-Vidal, M., Cui, H., 2016. Towards an Ediacaran Time Scale: problems, protocols, and prospects. Episodes 39 (4), 540–555.
Xiao, S., Zhang, Y., Knoll, A.H., 1998. Three-dimensional preservation of algae and animal embryos in a Neoproterozoic phosphorite. Nature 391, 553–558.
Xiao, S., Zhou, C., Liu, P., Wang, D., Yuan, X., 2014. Phosphatized acanthomorphic acritarchs and related microfossils from the Ediacaran Doushantuo Formation at Weng'an (South China) and their implications for biostratigraphic correlation. J. Paleontol. 88 (1), 1–67.
Yin, C., Liu, P., Awramik, S.M., Chen, S., Tang, F., Gao, L., Wang, Z., Riedman, L.A., 2011a. Acanthomorph Biostratigraphic Succession of the Ediacaran Doushantuo Formation in the East Yangtze Gorges, South China. Acta Geol. Sin. (Engl. Ed.) 85 (2), 283–295.
Yin, L., Wang, D., Yuan, X., Zhou, C., 2011b. Diverse small spinose acritarchs from the Ediacaran Doushantuo Formation, South China. Palaeoworld 20 (4), 279–289.
Yin, L., Zhu, M., Knoll, A.H., Yuan, X., Zhang, J., Hu, J., 2007. Doushantuo embryos preserved inside diapause egg cysts. Nature 446 (7136), 661–663.
Yuan, X., Chen, Z., Xiao, S., Zhou, C., Hua, H., 2011. An early Ediacaran assemblage of macroscopic and morphologically differentiated eukaryotes. Nature 470, 390–393.
Yuan, X., Hofmann, H.J., 1998. New microfossils from the Neoproterozoic (Sinian) Doushantuo Formation, Wengan, Guizhou Province, southwestern China. Alcheringa 22 (3), 189–222.
Zhang, S., Evans, D.A.D., Li, H., Wu, H., Jiang, G., Dong, J., Zhao, Q., Raub, T.D., Yang, T., 2013. Paleomagnetism of the late Cryogenian Nantuo Formation and paleogeographic implications for the South China Block. J. Asian Earth Sci. 72, 164–177.
Zhang, Y., Yin, L., Xiao, S., Knoll, A.H., 1998. Permineralized Fossils from the Terminal Proterozoic Doushantuo Formation, South China. J. Paleontol. Mem. Suppl. 72, 1–52.
Zhao, C., Li, X., Li, Z., Yu, Y., Zhang, H., Liu, A., 2012. Characteristics and geological significance of seismites of the Doushantuo Formation in Xikou, Hunan Province. Acta Sedimentol. Sin. 30 (6), 1032–1041.
Zhou, C., Brasier, M.D., Xue, Y., 2001. Three-dimensional phosphatic preservation of giant acritarchs from the terminal Proterozoic Doushantuo Formation in Guizhou and Hubei Provinces, South China. Palaeontology 44 (6), 1157–1178.
Zhou, C., Chen, Z., Xue, Y., 2002. New microfossils from the Late Neoproterozoic Doushantuo Formation at Chaoyang phosphorite deposit in Jiangxi Province, South China. Acta Palaeontol. Sin. 41 (2), 178–192.
Zhou, C., Jiang, S., Xiao, S., Chen, Z., Yuan, X., 2012. Rare earth elements and carbon isotope geochemistry of the Doushantuo Formation in South China: implication for middle Ediacaran shallow marine redox conditions. Chin. Sci. Bull. 57 (16), 1998–2006.
Zhou, C., Xiao, S., 2007. Ediacaran $\delta^{13}C$ chemostratigraphy of South China. Chem. Geol. 237 (1–2), 89–108.
Zhou, C., Xiao, S., Wang, W., Guan, C., Ouyang, Q., Chen, Z., 2017. The stratigraphic complexity of the middle Ediacaran carbon isotopic record in the Yangtze Gorges area, South China, and its implications for the age and chemostratigraphic significance of the Shuram excursion. Precambr. Res. 288, 23–38.
Zhou, C., Xie, G., McFadden, K.A., Xiao, S., Yuan, X., 2007. The diversification and extinction of Doushantuo-Pertatataka acritarchs in South China: causes and biostratigraphic significance. Geol. J. 42, 229–262.
Zhou, C., Yuan, X., Xiao, S., Chen, Z., Xue, Y., 2004. Phospatized fossil assemblage from the Doushantuo Formation in Baokang, Hubei Province. Acta Micropalaeontol. Sin. 21 (4), 349–366.
Zhu, M., Lu, M., Zhang, J., Zhao, F., Li, G., Yang, A., Zhao, X., Zhao, M., 2013. Carbon isotope chemostratigraphy and sedimentary facies evolution of the Ediacaran Doushantuo Formation in western Hubei, South China. Precambr. Res. 225, 7–28.
Zhu, M., Zhang, J., Yang, A., 2007. Integrated Ediacaran (Sinian) chronostratigraphy of South China. Palaeogeogr. Palaeoclimatol. Palaeoecol. 254 (1–2), 7–61.